

# Test of universality in the Ising spin glass using high temperature graph expansion

D. Daboul<sup>1,a</sup>, I. Chang<sup>2</sup>, and A. Aharony<sup>1</sup>

<sup>1</sup> School of Physics and Astronomy, Raymond and Beverly Sackler Faculty of Exact Sciences, Tel Aviv University, 69978 Tel Aviv, Israel

<sup>2</sup> Department of Physics, Pusan National University, Pusan 609-735, Korea

Received 22 July 2004

Published online 12 October 2004 – © EDP Sciences, Società Italiana di Fisica, Springer-Verlag 2004

**Abstract.** We calculate high-temperature graph expansions for the Ising spin glass model with 4 symmetric random distribution functions for its nearest neighbor interaction constants  $J_{ij}$ . Series for the Edwards-Anderson susceptibility  $\chi_{\text{EA}}$  are obtained to order 13 in the expansion variable  $(J/(k_{\text{B}}T))^2$  for the general  $d$ -dimensional hyper-cubic lattice, where the parameter  $J$  determines the width of the distributions. We explain in detail how the expansions are calculated. The analysis, using the Dlog-Padé approximation and the techniques known as M1 and M2, leads to estimates for the critical threshold  $(J/(k_{\text{B}}T_c))^2$  and for the critical exponent  $\gamma$  in dimensions 4, 5, 7 and 8 for all the distribution functions. In each dimension the values for  $\gamma$  agree, within their uncertainty margins, with a common value for the different distributions, thus confirming universality.

**PACS.** 05.70.Jk Critical point phenomena – 75.10.Nr Spin-glass and other random models

## 1 Introduction

In 1975, Edwards and Anderson (EA) [1] introduced a model for the theoretical study of spin glasses (SG) [2,3], which has started modern spin glass theory and has been of continued interest until today. Here we discuss the classical Ising case: The magnetic moments are represented by ‘spin’ variables  $\{s_i, i = 1, 2, \dots, N\}$ , which can assume the values  $s_i = \pm 1$  and are located on the sites  $\{i\}$  of the  $d$ -dimensional hyper-cubic lattice. During our calculations we use a finite number of lattice sites  $N$  but eventually we are interested in the thermodynamic limit,  $N \rightarrow \infty$ . The spins’ interaction is governed by the Hamiltonian

$$\mathcal{H}_{\{J_{ij}\}}(\{s_i\}) = - \sum_{\langle ij \rangle} J_{ij} s_i s_j - h_0 \sum_{i=1}^N s_i, \quad (1)$$

where  $\sum_{\langle ij \rangle}$  denotes the sum over all pairs of nearest neighbor lattice sites  $\langle ij \rangle$ , which we also call the lattice bonds, and the spin interaction constants  $J_{ij}$  are chosen at random from a symmetric probability distribution, which is the same for all bonds. The external magnetic field  $h_0$  is needed to define thermodynamic quantities as derivatives with respect to it, but apart from that, we concentrate on the case  $h_0 = 0$ . The Hamiltonian’s index  $\{J_{ij}\}$  indicates

that we deal with *quenched disorder*, i.e. the *thermodynamic average* for any observable is performed for a fixed set of coupling constants  $\{J_{ij}\}$ . The *configurational average* of measurable thermodynamic quantities, over the random variables, is performed subsequently. For self averaging quantities this leads to expressions of what could be measured in experiments. We denote the thermodynamic average of any observable  $A(\{s_i\})$  by  $\langle A \rangle_T$ , and the configurational average of any function  $X(\{J_{ij}\})$  by  $[X]_{\text{R}}$ .

The EA model neglects the details of the microscopic interaction between the spins, but exhibits the two essential ingredients that lead to the interesting features of spin glasses: *Quenched disorder* and *frustration*. Since little has been proved exactly for short ranged spin glass models, we assume what today is generally accepted, based on analytical and numerical evidence: Above the system’s lower critical dimension  $d_l$ , whose value is controversial but agreed to be between 2 and 3 [4,5], it undergoes a continuous transition at a non-zero critical temperature  $T_c$  to a low temperature spin glass phase. This phase is characterized by broken spin-flip symmetry, i.e. a non-zero *Edwards-Anderson order parameter*

$$q_{\text{EA}} = \frac{1}{N} \sum_{i=1}^N [\langle s_i \rangle_T^2]_{\text{R}}. \quad (2)$$

<sup>a</sup> e-mail: daboul@fractal.tau.ac.il

The upper critical dimension, above which mean field behavior becomes dominant, is believed to be  $d_u = 6$  [6, 7].

As the temperature  $T$  approaches  $T_c$  from above, we expect the susceptibility associated with  $q_{\text{EA}}$ , the *Edwards-Anderson susceptibility*,

$$\chi_{\text{EA}} = \frac{1}{N} \sum_{i,j=1}^N [\langle s_i s_j \rangle_T^2]_{\text{R}}, \quad (3)$$

to exhibit a power law divergence,  $\chi_{\text{EA}} \sim (T_c - T)^{-\gamma}$ , characterized by the critical exponent  $\gamma$ . In the present study we use series expansions to investigate this behavior. Both  $q_{\text{EA}}$  and  $\chi_{\text{EA}}$  are related to configurational averages of higher order logarithmic derivatives of the partition function  $-\frac{\partial^m \ln Z}{\partial h_0^m} \Big|_{h_0=0}$  with respect to the external magnetic field. Those relations become linear in the thermodynamic limit [8].

The renormalization group theory [9] in dimension  $d = 6 - \varepsilon$  predicts the universality of  $\gamma$  and of other exponents, related to it by scaling relations. The universality classes should be set by the dimensionalities of space and of the spin variables, and not by details of the distribution functions.

Series expansion has been used in the past to study the spin glass transition [8, 10–13] and the results support the statements mentioned above. Our renewed interest in the problem awoke with a series of studies [14–20] that found, based on computer simulations, that the critical exponents vary with the probability distribution for the quenched disorder in the coupling constants  $J_{ij}$ . This is in clear violation of universality and not sufficiently explained by theory.

Undoubtedly, many of the enormous complications and features observed in the study of spin glasses arise from the disorder inherent in these systems. They gave the model the reputation of being one of the toughest subjects in computational physics. Simulations are here directly impacted by long relaxation times, memory effects, hysteresis, the rugged energy landscape with many metastable states and the huge parameter space over which to average.

The technique of series expansion comes with two immediate advantages: The averaging over the randomness can be done *exactly*, and the series can, given the availability of graph data, be obtained in general dimension. The subsequent analysis is still done in each dimension separately, but results generally get more reliable with increasing dimension, while simulations become increasingly expensive in their computational demands. The previous series expansion studies of the Ising spin glass used only the bimodal random distribution of  $J_{ij} = \pm J$ , limiting their use in the comparison with the claims of violated universality. In the present study we extend the research by addressing several other symmetric distribution functions, each with a variable width determined by the parameter  $J$ . We use the same distributions as Bernardi and Campbell in [15], except for the exponential distribution, which is excluded for reasons given in Section 6. After

introducing additional notations and the random distribution functions in Section 2, we give a detailed explanation of the series generation in Sections 3 and 4, which should allow the interested reader to follow each step. As an example, we actually show the complete calculation of a fourth order series in Section 5. In Section 6 we present our general-dimension series in full, accompanied by some discussion of accuracy checks. Our series analysis and final results are described in Section 7 and we finish with our conclusions in Section 8.

## 2 Further notations and definitions

With  $\beta = \frac{1}{k_B T}$ , where  $k_B$  denotes Boltzmann's constant and  $T$  the absolute temperature, the ensemble average of an observable  $A$  is calculated by

$$\langle A \rangle_T = \frac{\text{Tr}(A e^{-\beta \mathcal{H}})}{Z} = \frac{\text{Tr}(A e^{-\beta \mathcal{H}})}{\text{Tr}(e^{-\beta \mathcal{H}})}, \quad (4)$$

where the partition function  $Z$  appears in the denominator. Here the trace ( $\text{Tr}$ ) is a shorthand for summing over all possible values of the spins'  $\{s_i\}$  configuration

$$\text{Tr} X = \text{Tr}_{\{s_i\}} X(\{s_i\}) = \sum_{s_1=\pm 1} \cdots \sum_{s_N=\pm 1} X(\{s_i\}). \quad (5)$$

The free energy per site  $F$  is obtained from  $Z$  by

$$F = \frac{1}{N} F_N \equiv -\frac{1}{\beta N} [\ln Z]_{\text{R}}. \quad (6)$$

Since the interaction constants  $J_{ij}$  appear only in products with  $\beta$ , it is convenient to use  $\kappa_{ij} = \beta J_{ij}$  as the argument of the distribution functions introduced below. If  $J^2$  is some measure of  $[J_{ij}^2]_{\text{R}}$ , then we also use  $\kappa = \beta J$  as expansion variable, at least temporarily. Since only even powers of  $\kappa$  remain, we eventually use  $x = \kappa^2$  as the expansion variable in our high temperature series. Likewise we use  $x_c = (J/(k_B T_c))^2$  to denote the *critical threshold*.

In the general case of a continuous probability distribution  $P(z)$ , the configurational average is the nested integral

$$[X]_{\text{R}} = \int_{-\infty}^{-\infty} \cdots \int_{-\infty}^{-\infty} X(\{z_{ij}\}) \prod_{\langle ij \rangle} (P(z_{ij}) dz_{ij}). \quad (7)$$

For the bimodal random distribution the coupling constants  $\kappa_{ij}$  for nearest neighbor pairs randomly assume only values of either  $+\kappa$  or  $-\kappa$ , so the latter integral can be written as the nested sum

$$[X]_{\text{R}} = \frac{1}{2^{Nd}} \sum_{\{\kappa_{(ij)} = \pm \kappa\}} X(\{\kappa_{ij}\}), \quad (8)$$

where a normalization factor of  $1/2$  stems from each  $\kappa_{ij}$  in the sum. In the  $d$ -dimensional hyper-cubic lattice with

$N$  sites the number of nearest neighbor pairs approaches  $Nd$  for large  $N$  when boundary effects become negligible.

Near the critical temperature  $T_c$ , the quantity of our interest,  $\chi_{EA}$ , is expected to have a singularity of the form

$$\chi_{EA} \approx A(x_c - x)^{-\gamma}(1 + B(x_c - x)^{\Delta_1} + \dots). \quad (9)$$

The aim of our analysis is to determine the critical exponent  $\gamma$  and, to a lesser extent, the first correction exponent  $\Delta_1$ . As for the free energy, we study this susceptibility per lattice site.

### 2.1 The random distributions

The different probability distributions, that we study, are listed below. We call them Bimodal, Gaussian, Uniform and Double-Triangular.

$$P_{\text{bim}}(z) = \frac{1}{2}(\delta[z - \kappa] + \delta[z + \kappa]) \quad (10)$$

$$P_{\text{gau}}(z) = \frac{e^{-\frac{z^2}{2\kappa^2}}}{\kappa\sqrt{2\pi}} \quad (11)$$

$$P_{\text{uni}}(z) = \begin{cases} 1/(2\kappa) & \text{for } |z| < \kappa \\ 0 & \text{for } |z| \geq \kappa \end{cases} \quad (12)$$

$$P_{\text{tri}}(z) = \begin{cases} |z|/\kappa^2 & \text{for } |z| < \kappa \\ 0 & \text{for } |z| \geq \kappa. \end{cases} \quad (13)$$

- The distributions are largely characterized by their moments

$$M_n \equiv [z^n]_{\text{R}} = \int_{-\infty}^{\infty} z^n P(z) dz. \quad (14)$$

- Since all distributions have the symmetry  $P(-z) = P(z)$ , the moments for odd  $n$  vanish. In particular, the distributions have zero mean  $[z]_{\text{R}} = \int_{-\infty}^{\infty} z P(z) dz = 0$ .
- For even  $n$  the moments are:  
 Bimodal distribution:  $\kappa^n$   
 Gaussian distribution:  $(n-1)!! \kappa^n$   
 Uniform distribution:  $\kappa^n/(n+1)$   
 Double-Triangular distribution:  $\kappa^n/(n/2+1)$ .
- Thus all the distributions are normalized  $\int_{-\infty}^{\infty} P(z) dz = 1$ .
- A distribution's second moment  $M_2 = \int_{-\infty}^{\infty} z^2 P(z) dz$ , equal to the variance, is commonly associated with its width. In all cases it is linear in  $\kappa^2$ , but with different pre-factors. Explicitly,  $M_2$  is equal to  $\kappa^2$  (Bimodal),  $\kappa^2$  (Gaussian),  $\kappa^2/3$  (Uniform), and  $\kappa^2/2$  (Double-Triangular), respectively. With slightly redefined variables,  $M_2$  could be equal to  $\kappa^2$  in all cases, which, in retrospective, would have been nicer.
- Figure 1 illustrates the distribution functions. The plots were calculated for the parameter  $\kappa = 5$ .

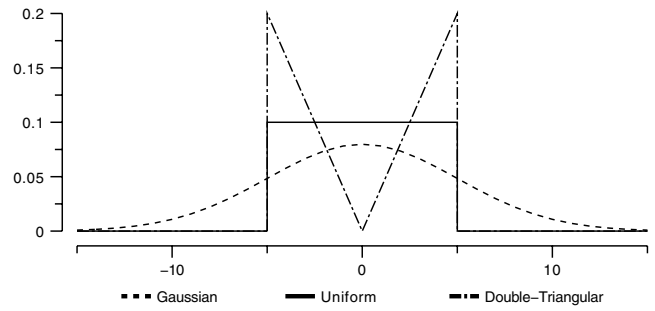


Fig. 1. The distribution functions for  $\kappa = 5$ .

### 2.2 Tangential moments

In the calculation of the series we encounter the following integrals over the distributions

$$m_n \equiv [k^n]_{\text{R}} = \int \tanh^n(z) P(z) dz. \quad (15)$$

We sometimes refer to  $m_n$  as the  $n$ th tangential moment of the distribution, in order to distinguish it from the regular moment (14). For a series to power  $\kappa^{2N}$  we need all moments up to  $m_N$  (not  $2N$  as we will see later). For the bimodal distribution the tangential moments are trivial:

$$m_n = \frac{1}{2}(\tanh^n(\kappa) + \tanh^n(-\kappa)) = \begin{cases} 0 & \text{odd } n \\ \tanh^n \kappa & \text{even } n. \end{cases}$$

The simple form  $m_{2n} = \tanh^{2n} \kappa = w^n$  makes  $w \equiv \tanh^2(\kappa)$  an alternative (and convenient) expansion variable for this case, which has been used in the past [8, 10]. This, however, is not true for the other distributions. For them it may be possible to calculate the  $m_n$  analytically, as well. But the results may be complicated functions of the parameter  $\kappa$ , not suitable for our power series expansion. Hence we are content to calculate the necessary moments  $m_n$  of all distributions as series in  $\kappa$ . To avoid the tedious work, this can conveniently be done with software for symbolic computation, such as Mathematica. The obtained coefficients are later used in the graph expansion, both for the computerized calculation and for the example in this article. The symmetry of the distributions makes all moments for odd  $n$  vanish. Due to the power series of  $\tanh^n \kappa$ , each moment  $m_n$  has only powers of  $\kappa^n$  and higher, somewhat important during cumulant subtraction. Note that in the framework of series expansions, this is an exact treatment of the randomness. We do not lose any additional information since a priori we are limited to the highest order of our final series.

As an illustration, we show the expansion of the first few moments for the bimodal and for the Gaussian distributions, to be used in the example below.

## 2.2.1 Bimodal tangential moments

$$m_0 = 1, \quad (16)$$

$$m_2 = \kappa^2 - \frac{2\kappa^4}{3} + \frac{17\kappa^6}{45} - \frac{62\kappa^8}{315} + \frac{1382\kappa^{10}}{14175} - \frac{21844\kappa^{12}}{467775} \\ + \frac{929569\kappa^{14}}{42567525} - \frac{6404582\kappa^{16}}{638512875} + \frac{443861162\kappa^{18}}{97692469875} - \frac{18888466084\kappa^{20}}{9280784638125} \\ + \frac{113927491862\kappa^{22}}{126109485376875} - \frac{58870668456604\kappa^{24}}{147926426347074375} + \frac{8374643517010684\kappa^{26}}{48076088562799171875} \\ - \frac{689005380505609448\kappa^{28}}{9086380738369043484375} + \frac{129848163681107301953\kappa^{30}}{3952575621190533915703125}, \quad (17)$$

$$m_4 = \kappa^4 - \frac{4\kappa^6}{3} + \frac{6\kappa^8}{5} - \frac{848\kappa^{10}}{945} + \frac{8507\kappa^{12}}{14175} \\ - \frac{3868\kappa^{14}}{10395} + \frac{46471426\kappa^{16}}{212837625} - \frac{47060768\kappa^{18}}{383107725} + \frac{518299498\kappa^{20}}{7753370625} \\ - \frac{92014385608\kappa^{22}}{2598619698675} + \frac{39319617599924\kappa^{24}}{2143861251406875} - \frac{12160377940064\kappa^{26}}{1304465840803125} \\ + \frac{14121349128787207129\kappa^{28}}{3028793579456347828125} - \frac{20894145609681223868\kappa^{30}}{9086380738369043484375}, \quad (18)$$

$$m_6 = \kappa^6 - 2\kappa^8 + \frac{37\kappa^{10}}{15} - \frac{2266\kappa^{12}}{945} + \frac{1901\kappa^{14}}{945} - \frac{79214\kappa^{16}}{51975} + \frac{136750052\kappa^{18}}{127702575} \\ - \frac{64742312\kappa^{20}}{91216125} + \frac{3282022\kappa^{22}}{7309575} - \frac{710423622556\kappa^{24}}{2598619698675} + \frac{82292419438259\kappa^{26}}{510443155096875} \\ - \frac{68433004067940682\kappa^{28}}{739632131735371875} + \frac{157107220075270779857\kappa^{30}}{3028793579456347828125}. \quad (19)$$

## 2.2.2 Gaussian tangential moments

$$m_0 = 1, \quad (20)$$

$$m_2 = \kappa^2 - 2\kappa^4 + \frac{17\kappa^6}{3} - \frac{62\kappa^8}{3} + \frac{1382\kappa^{10}}{15} - \frac{21844\kappa^{12}}{45} \\ + \frac{929569\kappa^{14}}{315} - \frac{6404582\kappa^{16}}{315} + \frac{443861162\kappa^{18}}{2835} - \frac{18888466084\kappa^{20}}{14175} \\ + \frac{1936767361654\kappa^{22}}{155925} - \frac{58870668456604\kappa^{24}}{467775} + \frac{8374643517010684\kappa^{26}}{6081075} \\ - \frac{689005380505609448\kappa^{28}}{42567525} + \frac{129848163681107301953\kappa^{30}}{638512875}, \quad (21)$$

$$m_4 = 3\kappa^4 - 20\kappa^6 + 126\kappa^8 - 848\kappa^{10} + \frac{93577\kappa^{12}}{15} \\ - 50284\kappa^{14} + \frac{46471426\kappa^{16}}{105} - \frac{800033056\kappa^{18}}{189} + \frac{9847690462\kappa^{20}}{225} \\ - \frac{92014385608\kappa^{22}}{189} + \frac{904351204798252\kappa^{24}}{155925} - \frac{12160377940064\kappa^{26}}{165} \\ + \frac{14121349128787207129\kappa^{28}}{14189175} - \frac{605930222680755492172\kappa^{30}}{42567525}, \quad (22)$$

$$m_6 = 15\kappa^6 - 210\kappa^8 + 2331\kappa^{10} - 24926\kappa^{12} + 271843\kappa^{14} \\ - 3089346\kappa^{16} + \frac{2324750884\kappa^{18}}{63} - \frac{20911766776\kappa^{20}}{45} \\ + 6173483382\kappa^{22} - \frac{16339743318788\kappa^{24}}{189} + \frac{1892725647079957\kappa^{26}}{1485} \\ - \frac{68433004067940682\kappa^{28}}{3465} + \frac{4556109382182852615853\kappa^{30}}{14189175}. \quad (23)$$

### 3 Connected graph expansion and cumulant subtraction

An extensive physical quantity  $X$  can be expanded in terms of connected graphs only [21]. To order  $n$  in a suitable expansion variable, say  $x$ , all connected graphs with  $n$  or less edges are used,

$$X = \sum_{b=0}^n \sum_{\Gamma \in \Gamma_b} w(\Gamma) X_{\Gamma}^c + O(|x|^{n+1}). \quad (24)$$

Here  $\Gamma_b$  denotes the set of all connected graphs  $\Gamma$  with  $b$  edges,  $w(\Gamma)$  is the lattice constant for weak embeddings of  $\Gamma$  inside the lattice (see Sect. 3.2) and  $X_{\Gamma}^c$  is the cumulant of the graph's contribution. For the quantity we calculate, the empty graph and the single vertex graph (with 0 edges) together only contribute a constant summand of 1 with the chosen normalization.

The cumulant contribution of a connected graph  $\Gamma$  is obtained by subtracting off the cumulant contribution of all its connected subgraphs,

$$X_{\Gamma}^c = X_{\Gamma} - \sum_{\gamma \subset \Gamma} X_{\gamma}^c. \quad (25)$$

Due to the subtractions,  $X_{\Gamma}^c$  is the contribution to  $X_{\Gamma}$ , which depends on every one of the  $b$  edges in  $\Gamma$  and thus has only terms of order  $b$  and higher in the expansion variable. This property allows us to stop the expansion at a certain size of graphs, with a series which is correct to the obtained order, and is in contrast to the original  $X_{\Gamma}$ , which can contribute to any power.

We often use the term *bond* instead of *edge* and likewise *site* instead of *vertex* since we deal with a physical model on a lattice, and will eventually embed the graph inside it. The physical model is also the reason we do not address digraphs or graphs with loops. Here the term *loop*, as commonly used in graph-theory, denotes an edge whose both ends are incident on the same vertex. This must be distinguished from a *cycle* (closed path) in the graph, which is important to us.

Our model involves only nearest-neighbor interactions, visualized by occupied lattice bonds. Since a graph  $\Gamma$  on the lattice is completely isolated from the rest of the infinite lattice by unoccupied bonds, the thermodynamics of its spins is determined by the reduced  $N_{\Gamma}$ -particle Hamiltonian for the graph

$$\mathcal{H}_{\Gamma}\{s_i \in \Gamma\} = - \sum_{\langle ij \rangle \in \Gamma} J_{ij} s_i s_j. \quad (26)$$

#### 3.1 Cumulant subtraction

Equation (25) contains the sum over connected subgraphs. In the following we have written out the cumulants for the smallest graphs, with explicit numerical coefficients and graph indices, because we will need them in the example later. For these small graphs, the expressions can easily

be confirmed by visual inspection using Figure 2. These cumulants are given by

$$\begin{aligned} X_{\Gamma_0}^c &= X_{\Gamma_0}, \\ X_{\Gamma_1}^c &= X_{\Gamma_1} - 2X_{\Gamma_0}^c, \\ X_{\Gamma_2}^c &= X_{\Gamma_2} - 3X_{\Gamma_0}^c - 2X_{\Gamma_1}^c, \\ X_{\Gamma_3}^c &= X_{\Gamma_3} - 4X_{\Gamma_0}^c - 3X_{\Gamma_1}^c - 3X_{\Gamma_2}^c, \\ X_{\Gamma_4}^c &= X_{\Gamma_4} - 4X_{\Gamma_0}^c - 3X_{\Gamma_1}^c - 2X_{\Gamma_2}^c, \\ X_{\Gamma_5}^c &= X_{\Gamma_5} - 4X_{\Gamma_0}^c - 4X_{\Gamma_1}^c - 4X_{\Gamma_2}^c - 4X_{\Gamma_4}^c, \\ X_{\Gamma_6}^c &= X_{\Gamma_6} - 5X_{\Gamma_0}^c - 4X_{\Gamma_1}^c - 3X_{\Gamma_2}^c - 2X_{\Gamma_4}^c, \\ X_{\Gamma_7}^c &= X_{\Gamma_7} - 5X_{\Gamma_0}^c - 4X_{\Gamma_1}^c - 4X_{\Gamma_2}^c - 1X_{\Gamma_3}^c - 2X_{\Gamma_4}^c, \\ X_{\Gamma_8}^c &= X_{\Gamma_8} - 5X_{\Gamma_0}^c - 4X_{\Gamma_1}^c - 6X_{\Gamma_2}^c - 4X_{\Gamma_3}^c. \end{aligned} \quad (27)$$

#### 3.2 The lattice constants for weak embeddings

In (24), the cumulant contribution of each graph is multiplied by its *lattice constant*  $w(\Gamma)$ . This constant is the number of distinct ways per lattice-site in which the graph can be weakly embedded in a particular lattice, and thus it ties our series to that specific lattice. In this article we address the  $d$ -dimensional hyper-cubic lattice, which, as the term suggests, is a generalization of the square lattice ( $d = 2$ ) and the cubic lattice ( $d = 3$ ). We use the tabulated functions  $w_{\Gamma}(d)$  from [22]. To calculate our example later on, we need the lattice constants of the first graphs:

$$\begin{aligned} w(\Gamma_0) &= 1, \\ w(\Gamma_1) &= d, \\ w(\Gamma_2) &= -d + 2d^2, \\ w(\Gamma_3) &= \frac{2d}{3} - 2d^2 + \frac{4d^3}{3}, \\ w(\Gamma_4) &= d - 4d^2 + 4d^3, \\ w(\Gamma_5) &= -\frac{d}{2} + \frac{d^2}{2}, \\ w(\Gamma_6) &= d + 4d^2 - 12d^3 + 8d^4, \\ w(\Gamma_7) &= -2d + 10d^2 - 16d^3 + 8d^4, \\ w(\Gamma_8) &= -\frac{d}{2} + \frac{11d^2}{6} - 2d^3 + \frac{2d^4}{3}. \end{aligned} \quad (28)$$

### 4 General calculation and simplifications for the Ising spin glass

The Boltzmann factor  $e^{-\beta\mathcal{H}}$  can be rewritten in a way that makes the calculation of the trace more convenient.

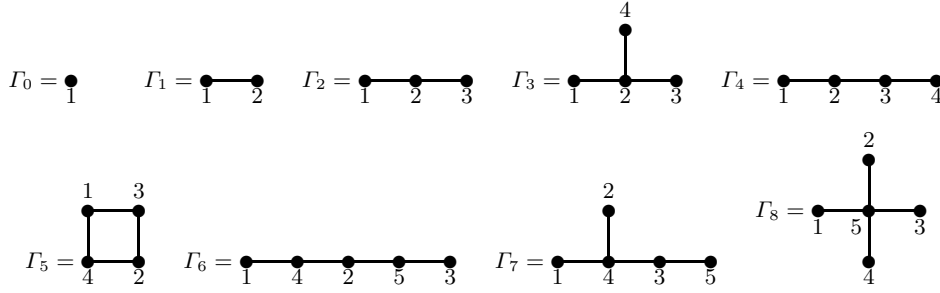


**Fig. 2.** The smallest graphs, that can be embedded into the hyper-cubic lattice.

With the notations  $\lambda = \beta h_0$ ,  $\tau = \tanh \lambda$ ,  $K_{ij} = \cosh \kappa_{ij}$  and  $k_{ij} = \tanh \kappa_{ij}$  we obtain:

$$\begin{aligned} e^{-\beta\mathcal{H}} &= \exp \left( \beta \sum_{\langle ij \rangle} J_{ij} s_i s_j + \beta h_0 \sum_{i=1}^N s_i \right) \\ &= \prod_{\langle ij \rangle} (\cosh(\kappa_{ij} s_i s_j) + \sinh(\kappa_{ij} s_i s_j)) \\ &\quad \times \prod_{i=1}^N (\cosh(\lambda s_i) + \sinh(\lambda s_i)). \end{aligned} \quad (29)$$

Now we exploit the fact that the only possible values of  $s_i$  are  $\pm 1$ , together with the symmetry of cosh and anti-symmetry of sinh:

$$e^{-\beta\mathcal{H}} = \cosh^N \lambda \prod_{\langle ij \rangle} K_{ij} \prod_{\langle ij \rangle} (1 + s_i s_j k_{ij}) \prod_{i=1}^N (1 + s_i \tau). \quad (30)$$

We address the case without external magnetic field,  $h_0 = 0$ , and call

$$Z_R = \frac{1}{2^N} \text{Tr} \left( \prod_{\langle ij \rangle} (1 + k_{ij} s_i s_j) \prod_{i=1}^N (1 + s_i \tau) \right) \quad (31)$$

the *reduced partition function* and sometimes use the notation  $Z_R(\Gamma_n) = Z_{\Gamma_n}$ . For the case of zero external magnetic field  $h_0 = 0$  we end up with the important (for our coming calculations) equation

$$\langle A \rangle_T = \frac{\text{Tr}_{\{s_i\}} \left( A \prod_{\langle ij \rangle} (1 + k_{ij} s_i s_j) \right)}{\text{Tr}_{\{s_i\}} \left( \prod_{\langle ij \rangle} (1 + k_{ij} s_i s_j) \right)}. \quad (32)$$

Often  $A$  will be a linear combination of  $s_m s_n$ . We will then see the terms

$$\langle s_m s_n \rangle_T = \frac{2^{-N} \text{Tr}_{\{s_i\}} \left( s_m s_n \prod_{\langle ij \rangle} (1 + k_{ij} s_i s_j) \right)}{2^{-N} \text{Tr}_{\{s_i\}} \left( \prod_{\langle ij \rangle} (1 + k_{ij} s_i s_j) \right)}. \quad (33)$$

#### 4.1 Graph-expansion for the Edwards-Anderson susceptibility

For the graph expansion of the Edwards-Anderson susceptibility (3) we apply the general formula (24). The calculation is done to order  $n$  in  $x = \kappa^2$ . With this expansion

variable all the dependence on the coupling strength parameter  $J$  and the temperature  $T$  are absorbed in the argument of the power series. We obtain

$$N \chi_{\text{EA}} = \sum_{b=0}^n \sum_{\Gamma \in \Gamma_b} w(\Gamma) X_{\Gamma}^c. \quad (34)$$

and also denote the associated (non-cumulant) observable on only one (sub)graph as

$$X_{\Gamma} = \sum_{i,j \in \Gamma} [\langle s_i s_j \rangle_T^2]_R. \quad (35)$$

## 5 Explicit calculation for the smallest graphs

We now show explicitly the calculation of  $\chi_{\text{EA}}$  for the smallest graphs in Figure 2, using the equations from the previous section. Here we often use  $[k_{ij}^n]_R = m_n$  following definition (15).

- For  $\Gamma_0$ , we have

$$\chi_{\text{EA}}(\Gamma_0) = 1 [\langle s_0^2 \rangle_T^2]_R = [\langle 1 \rangle_T^2]_R = 1. \quad (36)$$

For any spin, the self-correlation trivially equals 1.

- For  $\Gamma_1$ ,

$$\begin{aligned} \chi_{\text{EA}}(\Gamma_1) &= [\langle s_1 s_2 \rangle_T^2]_R + [\langle s_2 s_1 \rangle_T^2]_R + \langle s_1 \rangle^2 + \langle s_2 \rangle^2 \\ &= 2 [\langle s_1 s_2 \rangle_T^2]_R + 2. \end{aligned} \quad (37)$$

The denominator of  $\langle s_1 s_2 \rangle_T$  is

$$Z_{\Gamma_1} = Z_R(\Gamma_1) = 2^{-2} \text{Tr}_{\{s_1, s_2\}} (1 + k_{12} s_1 s_2) = 1, \quad (38)$$

and the numerator is

$$\begin{aligned} \langle s_1 s_2 \rangle_T Z_{\Gamma_1} &= 2^{-2} \text{Tr}_{\{s_1, s_2\}} (s_1 s_2 (1 + k_{12} s_1 s_2)) \\ &= 2^{-2} \text{Tr}_{\{s_1, s_2\}} (s_1 s_2 + k_{12}) = k_{12}. \end{aligned} \quad (39)$$

Thus,

$$\begin{aligned} \chi_{\text{EA}}(\Gamma_1) &= 2 [\langle s_1 s_2 \rangle_T^2]_R + 2 = 2 [k_{12}^2]_R + 2 \\ &= 2 [\tanh^2(\beta J_{12})]_R + 2 = 2m_2 + 2, \end{aligned} \quad (40)$$

where we used the definition of the tangential moment  $m_2$ .

- For  $\Gamma_2$ ,

$$\chi_{\text{EA}}(\Gamma_2) = 2 \left( [\langle s_1 s_2 \rangle_T^2]_{\text{R}} + [\langle s_2 s_3 \rangle_T^2]_{\text{R}} + [\langle s_1 s_3 \rangle_T^2]_{\text{R}} \right) + 3. \quad (41)$$

The denominator of each correlation is

$$\begin{aligned} Z_{\Gamma_2} &= 2^{-3} \text{Tr}_{\{s_1, s_2, s_3\}} \left( (1 + k_{12} s_1 s_2)(1 + k_{23} s_2 s_3) \right) \quad (42) \\ &= 2^{-3} \text{Tr}_{\{s_1, s_2, s_3\}} (1 + k_{12} s_1 s_2 + k_{23} s_2 s_3 + k_{12} k_{23} s_1 s_3) \\ &= 1. \end{aligned} \quad (43)$$

The numerator is

$$\langle s_1 s_2 \rangle_T Z_{\Gamma_2} = 2^{-3} \text{Tr}_{\{s_1, s_2, s_3\}} (s_1 s_2 (1 + k_{12} s_1 s_2) \times (1 + k_{23} s_2 s_3)) = k_{12}, \quad (44)$$

and likewise

$$\langle s_2 s_3 \rangle_T Z_{\Gamma_2} = k_{23}, \text{ and} \quad (45)$$

$$\langle s_1 s_3 \rangle_T Z_{\Gamma_2} = 2^{-3} \text{Tr}_{\{s_1, s_2, s_3\}} (s_1 s_3 (1 + k_{12} s_1 s_2) \times (1 + k_{23} s_2 s_3)) = k_{12} k_{23}. \quad (46)$$

The configurational average gives

$$[\langle s_1 s_2 \rangle_T^2]_{\text{R}} = [k_{12}^2]_{\text{R}} = m_2, \quad [\langle s_2 s_3 \rangle_T^2]_{\text{R}} = m_2 \quad (47)$$

and

$$[\langle s_1 s_3 \rangle_T^2]_{\text{R}} = [k_{12}^2 k_{23}^2]_{\text{R}} = [k_{12}^2]_{\text{R}} [k_{23}^2]_{\text{R}} = m_2^2, \quad (48)$$

where in the last step we used the fact that the random variables  $k_{ij}$  for different bonds are uncorrelated. Finally,

$$\chi_{\text{EA}}(\Gamma_2) = 3 + 4m_2 + 2m_2^2. \quad (49)$$

A few general observations are in order: From the possible values of a spin variable,  $s_i = \pm 1$ , we trivially have  $s_i^2 = 1$ . Further, the trace sums over the possible values of each spin, so any summand with an unpaired  $s_i$  vanishes. When writing out the product within the traces  $(1 + k_{ij} s_i s_j) \cdots (1 + k_{kl} s_k s_l)$  one has to choose from each pair of  $\langle ij \rangle$  (and for any resulting summand) either the constant 1 or the bond factor  $k_{ij}$ . To find the terms that will actually survive the trace, the  $s_i s_j$  site-factors accompanying any bond have to be combined with other sites, either from another bond in the graph or from terms originally present inside the trace.

For any acyclic graph, which we have seen so far, we immediately see that the reduced partition function is always equal to 1; no bond can be combined with others to eliminate all unpaired sites. Also the numerator for pair correlations remains simple. Visually only a path of bonds joining the two sites in question yields factors of only paired spins, which survive the trace. Each such bond contributes a factor of  $m_2$ . A constant multiplier results from the number of ways the pair of sites (and equivalent

pairs) can be joined. For cyclic graphs the calculation becomes much more complicated. In passing please note that one of the inherent features of spin glasses is *frustration*. Only a cyclic graph is susceptible to this phenomenon and as such can possibly integrate true SG-properties into our series.

- For  $\Gamma_3$ ,

$$\begin{aligned} \chi_{\text{EA}}(\Gamma_3) &= 2 \left[ \langle s_1 s_2 \rangle_T^2 + \langle s_2 s_3 \rangle_T^2 + \langle s_2 s_4 \rangle_T^2 + \langle s_1 s_3 \rangle_T^2 \right. \\ &\quad \left. + \langle s_1 s_4 \rangle_T^2 + \langle s_3 s_4 \rangle_T^2 \right]_{\text{R}} + 4 \\ &= 4 + 6m_2 + 6m_2^2. \end{aligned} \quad (50)$$

- For  $\Gamma_4$ ,

$$\begin{aligned} \chi_{\text{EA}}(\Gamma_4) &= 2 \left( [\langle s_1 s_2 \rangle_T^2]_{\text{R}} + [\langle s_2 s_3 \rangle_T^2]_{\text{R}} + [\langle s_3 s_4 \rangle_T^2]_{\text{R}} \right. \\ &\quad \left. + [\langle s_1 s_3 \rangle_T^2]_{\text{R}} + [\langle s_2 s_4 \rangle_T^2]_{\text{R}} + [\langle s_1 s_4 \rangle_T^2]_{\text{R}} \right) \\ &\quad + 4 \\ &= 4 + 6m_2 + 4m_2^2 + 2m_2^3. \end{aligned} \quad (51)$$

- For  $\Gamma_5$ ,

$$\chi_{\text{EA}}(\Gamma_5) = 4 + 8 [\langle s_1 s_3 \rangle_T^2]_{\text{R}} + 4 [\langle s_1 s_2 \rangle_T^2]_{\text{R}}. \quad (52)$$

Here we used the equivalence of *pairs of sites*, in terms of adjacencies, to reduce the number of terms to 3. We defer calculation of the result till later.

- For  $\Gamma_6$ ,

$$\begin{aligned} \chi_{\text{EA}}(\Gamma_6) &= 2 \left[ 4 \langle s_1 s_4 \rangle_T^2 + 3 \langle s_1 s_2 \rangle_T^2 + 2 \langle s_1 s_5 \rangle_T^2 \right. \\ &\quad \left. + 1 \langle s_1 s_3 \rangle_T^2 \right]_{\text{R}} + 5 = 5 + 8m_2 + 6m_2^2 + 4m_2^3 + 2m_2^4. \end{aligned} \quad (53)$$

- For  $\Gamma_7$ ,

$$\begin{aligned} \chi_{\text{EA}}(\Gamma_7) &= 2 \left[ 4 \langle s_1 s_4 \rangle_T^2 + 4 \langle s_1 s_2 \rangle_T^2 + 2 \langle s_1 s_5 \rangle_T^2 \right]_{\text{R}} \\ &\quad + 5 = 5 + 8m_2 + 8m_2^2 + 4m_2^3. \end{aligned} \quad (54)$$

- For  $\Gamma_8$ ,

$$\begin{aligned} \chi_{\text{EA}}(\Gamma_8) &= 2 \left[ 4 \langle s_1 s_5 \rangle_T^2 + 6 \langle s_1 s_2 \rangle_T^2 \right]_{\text{R}} \\ &\quad + 5 = 5 + 8m_2 + 12m_2^2. \end{aligned} \quad (55)$$

We now resume the calculation of  $\chi_{\text{EA}}(\Gamma_5)$  from (52) which, due to the graph's cycle, is significantly more complicated than the contribution of the other graphs. The complexity enters through the non-trivial partition function

$$\begin{aligned} Z_{\Gamma_5} &= 2^{-4} \text{Tr}_{\{s_1, s_2, s_3, s_4\}} \left( (1 + k_{13} s_1 s_3)(1 + k_{23} s_2 s_3) \right. \\ &\quad \left. \times (1 + k_{14} s_1 s_4)(1 + k_{24} s_2 s_4) \right) = 1 + k_{13} k_{23} k_{14} k_{24}. \end{aligned} \quad (56)$$

The numerators for the spin correlations are  $\langle s_1 s_3 \rangle_T Z_{\Gamma_5} = k_{13} + k_{14} k_{24} k_{23}$  and  $\langle s_1 s_2 \rangle_T Z_{\Gamma_5} = k_{13} k_{23} + k_{14} k_{24}$ . The complicated part is now performing the averaging over the randomness for

$$[\langle s_1 s_3 \rangle_T^2]_{\text{R}} = \left[ \left( \frac{k_{13} + k_{14} k_{24} k_{23}}{1 + k_{13} k_{23} k_{14} k_{24}} \right)^2 \right]_{\text{R}} \quad (57)$$

and

$$[\langle s_1 s_2 \rangle_T^2]_{\text{R}} = \left[ \left( \frac{k_{13} k_{23} + k_{14} k_{24}}{1 + k_{13} k_{23} k_{14} k_{24}} \right)^2 \right]_{\text{R}}. \quad (58)$$

In fact, for most probability distributions we do not know to calculate this directly. For the bimodal distribution it is possible, and was in fact done also for much larger graphs with a computer [8]. For continuous distributions the calculation would at best become extremely tedious and most likely not feasible for large graphs. Our solution again utilizes a power expansion. By this we do not lose any more information since our final series are limited to a certain order in the expansion variable anyway.

To make the expansion process more obvious we rewrite the equations with the symbols  $u_{ij} = k_{ij}/k$  such that  $k_{ij} = k u_{ij}$  and

$$\langle s_1 s_3 \rangle_T = \frac{k u_{13} + k^3 u_{14} u_{23} u_{24}}{1 + k^4 u_{13} u_{23} u_{14} u_{24}}, \quad (59)$$

$$\langle s_1 s_2 \rangle_T = \frac{k^2 u_{13} u_{23} + k^2 u_{14} u_{24}}{1 + k^4 u_{13} u_{23} u_{14} u_{24}}, \quad (60)$$

and expand the squares in powers of  $k$ :

$$\begin{aligned} \langle s_1 s_3 \rangle_T^2 &= u_{13}^2 k^2 + 2 u_{13} u_{14} u_{23} u_{24} k^4 \\ &+ (-2 u_{13}^3 u_{14} u_{23} u_{24} + u_{14}^2 u_{23}^2 u_{24}^2) k^6 - 4 (u_{13}^2 u_{14}^2 u_{23}^2 u_{24}^2) k^8 \\ &+ (3 u_{13}^4 u_{14}^2 u_{23}^2 u_{24}^2 - 2 u_{13} u_{14}^3 u_{23}^3 u_{24}^3) k^{10} + 6 u_{13}^3 u_{14}^3 u_{23}^3 u_{24}^3 k^{12} \\ &+ (-4 u_{13}^5 u_{14}^3 u_{23}^3 u_{24}^3 + 3 u_{13}^2 u_{14}^4 u_{23}^4 u_{24}^4) k^{14} + O(|k|^{15}), \end{aligned} \quad (61)$$

$$\begin{aligned} \langle s_1 s_2 \rangle_T^2 &= k^4 (u_{13}^2 u_{23}^2 + 2 u_{13} u_{14} u_{23} u_{24} + u_{14}^2 u_{24}^2) \\ &+ k^8 (-2 u_{13}^3 u_{14} u_{23}^3 u_{24} - 4 u_{13}^2 u_{14}^2 u_{23}^2 u_{24}^2 \\ &- 2 u_{13} u_{14}^3 u_{23}^3 u_{24}^3) + k^{12} (3 u_{13}^4 u_{14}^2 u_{23}^2 u_{24}^2 \\ &+ 6 u_{13}^3 u_{14}^3 u_{23}^3 u_{24}^3 + 3 u_{13}^2 u_{14}^4 u_{23}^2 u_{24}^4) + O(|k|^{15}). \end{aligned} \quad (62)$$

With the fractions removed, we can again factorize for averages over independent variables, and thus use the previously defined moments of the random distributions:

$$[\langle s_1 s_3 \rangle_T^2]_{\text{R}} = m_2 + m_2^3 - 4 m_2^4 + 3 m_2^3 m_4 + 3 m_2 m_4^3 + O(|\kappa|^{15}), \quad (63)$$

$$[\langle s_1 s_2 \rangle_T^2]_{\text{R}} = 2 m_2^2 - 4 m_2^4 + 6 m_2^2 m_4^2 + O(|\kappa|^{15}). \quad (64)$$

Here we expanded to a higher power than actually necessary for the largest graph that we consider in this example. It shows that higher moments actually show up. We first encountered  $m_3 = m_5 = 0$  and

$$m_4 = [k_{ij}^4]_{\text{R}} = [\tanh^4 \kappa_{ij}]_{\text{R}} = \int \tanh^4 x P(x) dx. \quad (65)$$

For the bimodal distribution we can quickly use the simple form of the moments  $m_2 = w$  and  $m_4 = w^2$ , and obtain

$$[\langle s_1 s_3 \rangle_T^2]_{\text{R}} = w + w^3 - 4 w^4 + 3 w^5 + 3 w^7 + \dots \quad (66)$$

$$[\langle s_1 s_2 \rangle_T^2]_{\text{R}} = 2 w^2 - 4 w^4 + 6 w^6 + \dots, \quad (67)$$

and thus

$$\begin{aligned} \chi_{\text{EA}}(\Gamma_5) &= 4 + 8w + 8w^2 + 8w^3 - 48w^4 + 24w^5 \\ &+ 24w^6 + 24w^7 + O(|w|^8). \end{aligned} \quad (68)$$

For the general distribution we remain with

$$\begin{aligned} \chi_{\text{EA}}(\Gamma_5) &= 4 + 8(m_2 + m_2^2 + m_2^3 - 6m_2^4 + 3m_2^3 m_4 \\ &+ 3m_2^2 m_4^2 + 3m_2 m_4^3) + O(|\kappa|^{15}), \end{aligned} \quad (69)$$

on which we elaborate further.

## 5.1 Performing cumulant subtraction

In this section we perform the cumulant subtraction for the quantity  $\chi_{\text{EA}}$ , which we calculated in the previous section. The general equations were given in Section 3.1 and in the following we show the cumulant graph contributions first in terms of the tangential moments and also for the case of the bimodal distribution using  $w$  as the expansion variable, thus substituting  $m_2 = w$  and  $m_4 = w^2$ .

$$\begin{aligned} X_{\Gamma_0}^c &= 1, \\ X_{\Gamma_1}^c &= 2m_2 = 2w, \\ X_{\Gamma_2}^c &= 2m_2^2 = 2w^2, \\ X_{\Gamma_3}^c &= 0, \\ X_{\Gamma_4}^c &= 2m_2^3 = 2w^3, \\ X_{\Gamma_5}^c &= -48m_2^4 + 24m_2^3 m_4 + 24m_2^2 m_4^2 + 24m_2 m_4^3 + \dots \\ &= -48w^4 + 24w^5 + 24w^6 + 24w^7 + \dots, \\ X_{\Gamma_6}^c &= 2m_2^4 = 2w^4, \\ X_{\Gamma_7}^c &= 0, \\ X_{\Gamma_8}^c &= 0. \end{aligned} \quad (70)$$

Indeed we see that no graph contributes to a power of  $w$  less than its number of bonds. This fact is used in the computerized calculation as an internal check.

In general we use  $\kappa$  (or  $x = \kappa^2$ ) as the expansion variable, for which we now use the expansions of the moments  $m_n$  from Section 2.2. We show the result for the Gaussian distribution:

$$\begin{aligned} X_{\Gamma_0}^c &= 1, \\ X_{\Gamma_1}^c &= 2\kappa^2 - 4\kappa^4 + \frac{34\kappa^6}{3} - \frac{124\kappa^8}{3} + O(|\kappa|^{10}), \\ X_{\Gamma_2}^c &= 2\kappa^4 - 8\kappa^6 + \frac{92\kappa^8}{3} + O(|\kappa|^{10}), \\ X_{\Gamma_3}^c &= 0, \\ X_{\Gamma_4}^c &= 2\kappa^6 - 12\kappa^8 + O(|\kappa|^{10}), \\ X_{\Gamma_5}^c &= -48\kappa^8 + O(|\kappa|^{10}), \\ X_{\Gamma_6}^c &= 2\kappa^8 + O(|\kappa|^{10}), \\ X_{\Gamma_7}^c &= 0, \\ X_{\Gamma_8}^c &= 0. \end{aligned} \quad (71)$$



## 5.2 Using the lattice constants

Using (24) together with the lattice constants of the smallest graphs, as given in Section 3.2, we can now perform the final summation and obtain the series. For the Gaussian distribution, we find

$$\begin{aligned}\chi_{\text{EA}} &= 1 + 2d\kappa^2 + (-6d + 4d^2)\kappa^4 \\ &+ \left(\frac{64d}{3} - 24d^2 + 8d^3\right)\kappa^6 \\ &+ \left(-58d + \frac{280d^2}{3} - 72d^3 + 16d^4\right)\kappa^8 + \dots\end{aligned}\quad (72)$$

For the bimodal distribution one has

$$\begin{aligned}\chi_{\text{EA}} &= 1 + 2d\kappa^2 + \left(-\frac{10d}{3} + 4d^2\right)\kappa^4 \\ &+ \left(\frac{244d}{45} - \frac{40d^2}{3} + 8d^3\right)\kappa^6 \\ &+ \left(\frac{1210d}{63} + \frac{24d^2}{5} - 40d^3 + 16d^4\right)\kappa^8 + \dots\end{aligned}\quad (73)$$

or, expanded in  $w$ ,

$$\begin{aligned}\chi_{\text{EA}} &= 1 + 2dw + (-2d + 4d^2)w^2 + (2d - 8d^2 + 8d^3)w^3 \\ &+ (26d - 16d^2 - 24d^3 + 16d^4)w^4 + \dots\end{aligned}\quad (74)$$

## 6 The full series

The series for the  $d$ -dimensional hyper-cubic lattice to order 13 need to take into account 20724 graphs of up to 13 edges, and are hence calculated using computers. We use the graph data files that were originally prepared for [22] by Wan et al., and have since been used in many studies. Programs were written, that use these data files to compute the series as outlined in the previous sections. Details of the algorithms, including important efficiency considerations, are presented in [23].

Tables 1 to 4 show the resulting series in full. In Table 1, for the bimodal distribution, the coefficients are given as exact fractions. For the other distributions they were in part calculated using the data type *long double* in C++ which limits their accuracy. For comparison we used two different processor architectures where this data type is represented in either 96 or 128 bits, and also compared part of the data with calculations done in double precision (64 bits). Small rounding errors are obvious in most numbers, but further investigation shows, that for coefficients large in absolute value, the numerical accuracies become important. Originally we had included in this work the *exponential random distribution* which is also addressed in [15]. This distribution decays slower than the others

and the resulting coefficients become very large in absolute value, to a degree that intermediate numbers either can not be presented in long double variables or the rounding errors become so dominant that the highest order coefficients come out completely wrong. We have started to calculate the series using arbitrary-precision numerical libraries, but that work was not ready in time to be included here. We exclude the exponential distribution from the present work, and for the remaining series present the coefficients in as many digits as we expect to be correct from the comparisons mentioned above.

From experience we know that small changes in the coefficients do not influence the results obtained from series analysis. Hence the numerical inaccuracies present in the power series should not influence our final results. For the bimodal distribution we supplement coefficients for orders  $x^{14}$  and  $x^{15}$ , which were calculated using the non-free-end (NFE) technique and associated graph data. In this technique by Harris [24] the thermodynamic functions under study are renormalized in such a way that the contribution from a graph with at least one free end (i.e. a vertex with only one incident edge) vanishes. This renormalization is possible for the bimodal distribution [8] but was not obtained for the others. We use equations from [8] for the NFE-expansion in  $w$ , but do not describe the process here since the series can also be obtained directly by variable transformation from  $w$  to  $x$ , which indeed we use as a consistency check.

Several checks are performed to assure the correctness of our series expansions: The first is a complete recalculation of the corresponding series in [8] for the bimodal distribution, which shows that the algorithm and its implementation are basically correct.

We mentioned earlier that after cumulant subtraction, a graph of  $b$  edges has only terms of order  $b$  and higher in the expansion variable. As an additional check we do the actual calculation of the vanishing terms, track the maximal deviation from zero, and confirm that this number is in the same range as the numerical rounding errors observed elsewhere.

For a few sequences of coefficients we find, by examination of the numerical values, what their exact value must be in general. If we denote by  $a_{ij}$  the coefficient multiplying  $x^i d^j$  we observe:

- For the bimodal distribution  $a_{ii} = 2^i$  and  $a_{i,(i-1)} = -(5/6)2^i(i-1)$ .
- For the Gaussian distribution  $a_{ii} = 2^i$  and  $a_{i,(i-1)} = -(3/2)2^i(i-1)$ .
- For the uniform distribution  $a_{ii} = (2/3)^i$  and  $a_{i,(i-1)} = -(11/10)(2/3)^i(i-1)$ .
- For the double-triangular distribution  $a_{ii} = 1$  and  $a_{i,(i-1)} = -(17/18)(i-1)$ .

Obviously this is no rigorous check from first principles, but if we believe in the regularity and that we can at least calculate the first few orders correctly, it adds confidence that no mistake was done at higher orders and that the numerical errors are not exceedingly large. A more comprehensive check for numerical rounding errors was already mentioned above in this section.

**Table 1.** Series for the Bimodal distribution on the  $d$ -dimensional hyper-cubic lattice and for  $x = (J/k_{\text{B}}T)^2$ .

Terms of the series. $\chi_{\text{EA}} = 1 + \dots$	
$+2 x^1 d^1$	
$-\frac{10}{3} x^2 d^1$	$+4 x^2 d^2$
$+\frac{244}{45} x^3 d^1$	$-\frac{40}{3} x^3 d^2$
$+8 x^3 d^3$	
$+\frac{1210}{63} x^4 d^1$	$+\frac{24}{5} x^4 d^2$
$-40 x^4 d^3$	$+16 x^4 d^4$
$-\frac{2557316}{14175} x^5 d^1$	$+\frac{44480}{189} x^5 d^2$
$+\frac{296}{15} x^5 d^3$	$-\frac{320}{3} x^5 d^4$
$+32 x^5 d^5$	
$+\frac{15891824}{93555} x^6 d^1$	$-\frac{9373372}{14175} x^6 d^2$
$+\frac{111488}{189} x^6 d^3$	$+\frac{4688}{45} x^6 d^4$
$-\frac{800}{3} x^6 d^5$	$+64 x^6 d^6$
$+\frac{190090194848}{42567525} x^7 d^1$	$-\frac{13641704}{2079} x^7 d^2$
$+\frac{645088}{945} x^7 d^3$	$+\frac{283264}{189} x^7 d^4$
$+\frac{1280}{3} x^7 d^5$	$-640 x^7 d^6$
$+128 x^7 d^7$	
$-\frac{545049148646}{127702575} x^8 d^1$	$+\frac{3811431542104}{212837625} x^8 d^2$
$-\frac{32973784}{2079} x^8 d^3$	$-\frac{7834448}{4725} x^8 d^4$
$+\frac{229856}{63} x^8 d^5$	$+\frac{22016}{15} x^8 d^6$
$-\frac{4480}{3} x^8 d^7$	$+256 x^8 d^8$
$-\frac{2171514982687276}{8881133625} x^9 d^1$	$+\frac{35779921623392}{76621545} x^9 d^2$
$-\frac{32560925165624}{127702575} x^9 d^3$	$+\frac{3151565216}{93555} x^9 d^4$
$-\frac{31525376}{2835} x^9 d^5$	$+\frac{1574144}{189} x^9 d^6$
$+\frac{203392}{45} x^9 d^7$	$-\frac{10240}{3} x^9 d^8$
$+512 x^9 d^9$	
$-\frac{202257782879679928}{1856156927625} x^{10} d^1$	$-\frac{3150596158319108}{7753370625} x^{10} d^2$
$+\frac{17497504604224}{18243225} x^{10} d^3$	$-\frac{44042569593584}{91216125} x^{10} d^4$
$+\frac{255487168}{4455} x^{10} d^5$	$-\frac{28463552}{675} x^{10} d^6$
$+\frac{474880}{27} x^{10} d^7$	$+\frac{193792}{15} x^{10} d^8$
$-7680 x^{10} d^9$	$+1024 x^{10} d^{10}$
$+\frac{44286591649508625456608}{2143861251406875} x^{11} d^1$	$-\frac{24516788251206488696}{519723939735} x^{11} d^2$
$+\frac{2975087273749088}{80405325} x^{11} d^3$	$-\frac{491320094394464}{42567525} x^{11} d^4$
$+\frac{14408475958592}{14189175} x^{11} d^5$	$+\frac{753069824}{6237} x^{11} d^6$
$-\frac{270251392}{2025} x^{11} d^7$	$+\frac{6347776}{189} x^{11} d^8$
$+\frac{175104}{5} x^{11} d^9$	$-\frac{51200}{3} x^{11} d^{10}$
$+2048 x^{11} d^{11}$	
$+\frac{102687986431081211931032}{2275791174570375} x^{12} d^1$	$-\frac{98234614240598344870804}{2143861251406875} x^{12} d^2$
$-\frac{1631193202018689472}{39978764595} x^{12} d^3$	$+\frac{132365195242707824}{2170943775} x^{12} d^4$
$-\frac{36568729916000}{1702701} x^{12} d^5$	$+\frac{5544027735104}{2837835} x^{12} d^6$
$+\frac{96053248}{297} x^{12} d^7$	$-\frac{24126464}{63} x^{12} d^8$
$+\frac{3447296}{63} x^{12} d^9$	$+\frac{821248}{9} x^{12} d^{10}$
$-\frac{112640}{3} x^{12} d^{11}$	$+4096 x^{12} d^{12}$
$-\frac{110468581411293350924457444112}{48076088562799171875} x^{13} d^1$	$+\frac{172781445528971814087368}{28988129795625} x^{13} d^2$
$-\frac{2939279178242203350187328}{510443155096875} x^{13} d^3$	$+\frac{4778773293081621239776}{1856156927625} x^{13} d^4$
$-\frac{23565892697470112}{46990125} x^{13} d^5$	$+\frac{5353769766272}{289575} x^{13} d^6$

Terms of the series. $\chi_{EA} = 1 + \dots$	
$+\frac{39918090277888}{10135125} x^{13} d^7$	$+\frac{688011776}{693} x^{13} d^8$
$-\frac{179936768}{175} x^{13} d^9$	$+\frac{1286144}{21} x^{13} d^{10}$
$+\frac{1153024}{5} x^{13} d^{11}$	$-81920 x^{13} d^{12}$
$+8192 x^{13} d^{13}$	
$-\frac{305463146085574972582952872664}{33041384503160158125} x^{14} d^1$	$+\frac{50334647726118167100558221079016}{3028793579456347828125} x^{14} d^2$
$-\frac{824015715606745029679283608}{147926426347074375} x^{14} d^3$	$-\frac{157096153765758568475862928}{32157918771103125} x^{14} d^4$
$+\frac{30648160725228437701792}{7795859096025} x^{14} d^5$	$-\frac{2624211856887202496}{2960377875} x^{14} d^6$
$+\frac{43529789374208}{1563705} x^{14} d^7$	$+\frac{1037253983072768}{127702575} x^{14} d^8$
$+\frac{1206767104}{385} x^{14} d^9$	$-\frac{1487067136}{567} x^{14} d^{10}$
$-\frac{5660672}{189} x^{14} d^{11}$	$+\frac{8531968}{15} x^{14} d^{12}$
$-\frac{532480}{3} x^{14} d^{13}$	$+16384 x^{14} d^{14}$
$+\frac{129382646873333294113597991611697536}{3952575621190533915703125} x^{15} d^1$	$-\frac{338533911194409672724356315499808}{363455229534761739375} x^{15} d^2$
$+\frac{3142897456730380314538798434325456}{3028793579456347828125} x^{15} d^3$	$-\frac{257903955006958171637687615776}{443779279041223125} x^{15} d^4$
$+\frac{5449914292983317242598754368}{32157918771103125} x^{15} d^5$	$-\frac{67310752760322121480064}{2998407344625} x^{15} d^6$
$+\frac{11493150389809720832}{23260111875} x^{15} d^7$	$+\frac{4618407513611776}{127702575} x^{15} d^8$
$+\frac{3526208986206208}{212837625} x^{15} d^9$	$+\frac{904493910016}{93555} x^{15} d^{10}$
$-\frac{90834735104}{14175} x^{15} d^{11}$	$-\frac{93716480}{189} x^{15} d^{12}$
$+\frac{61898752}{45} x^{15} d^{13}$	$-\frac{1146880}{3} x^{15} d^{14}$
$+32768 x^{15} d^{15}$	

## 7 Analysis of the series

Our analysis uses the Dlog-Padé method [25] and the methods M1 and M2 [26,27]. Each of these is combined with Euler-transformations for improved results. For each series, our main goal is to obtain the critical value  $x_c$  and the critical exponent  $\gamma$  which describe the power law divergence, as in

$$\chi_{EA} \approx A(x_c - x)^{-\gamma}(1 + B(x_c - x)^{\Delta_1}). \quad (75)$$

The series analysis is done for a fixed dimension at a time. We present our results for dimensions 7 and 8 above the upper critical dimension and for 5 and 4 below it. We also attempted an analysis in the physical dimension 3 but the results are not conclusive.

At the upper critical dimension  $d_c = 6$  the corrections to scaling become logarithmic and there one expects the general form

$$\chi_{EA}(x) \approx A(x_c - x)^{-\gamma} |\ln(x_c - x)|^\theta. \quad (76)$$

Instead of M1 and M2, one can apply a modified method to take such corrections into account. This was pursued in [8], for the Bimodal distribution, but the authors reported poor convergence already for that case. Given that our series for the other distributions are more problematic, we did not attempt a detailed analysis in  $d = 6$ .

It is generally observed in series analysis, that for a given order of expansion, a series behaves better, the higher the dimension. That is also the case in the study at hand. Qualitatively it is understood by the fast increase of

the embedding constants with increasing dimension. Thus a much larger number of lattice configurations contributes to the higher dimensional series, allowing it to capture more of the underlying Physics.

### 7.1 Dlog-Padé analysis

The Dlog-Padé method is one of the most common methods for the asymptotic analysis of power series. One calculates Padé approximants to the logarithmic derivative of the series and obtains estimates for the critical value  $x_c$  of the expansion variable  $x$  (the threshold) and for the critical exponent  $\gamma$  from their real first order poles and the corresponding residues. We also refer to the pole-residue pairs as data-points since we often plot them in diagrams of residues versus poles.

Many series point to singularities other than those representing the physical critical point. They are observed in the Dlog-Padé analysis of the original series and, depending on their strength and location in the complex plane, hamper convergence of the data points. This effect appears to be strongest when an extra singularity is on the negative real axis closer to the origin than the physical one. Application of an Euler-transformation into the new variable  $z = x_n x / (x_n - x)$ , with  $x_n$  at or close to the disturbing singularity, usually improves the behavior of the transformed series.

For some series, in particular those in higher dimension, we obtain satisfactory results in this manner. Data points in the pole-residue plots are high in number and

**Table 2.** Series for the Gaussian distribution on the  $d$ -dimensional hyper-cubic lattice and for  $x = (J/k_B T)^2$ .

Terms of the series. $\chi_{EA} = 1 + \dots$		
<hr/>		
$+2 x^1 d^1$		
<hr/>		
$-6 x^2 d^1$		$+4 x^2 d^2$
<hr/>		
$+21.3333333333333333 x^3 d^1$	$-24 x^3 d^2$	$+8 x^3 d^3$
<hr/>		
$-57.9999999999999999 x^4 d^1$	$+93.3333333333333333 x^4 d^2$	$-71.9999999999999999 x^4 d^3$
<hr/>		
$+15.9999999999999999 x^4 d^4$		
<hr/>		
$+20.2666666666666666 x^5 d^1$	$-119.9999999999999999 x^5 d^2$	$+359.9999999999999999 x^5 d^3$
<hr/>		
$-192 x^5 d^4$		$+32 x^5 d^5$
<hr/>		
$+558.40000000000000 x^6 d^1$	$-934.48888888888888 x^6 d^2$	$-991.99999999999999 x^6 d^3$
<hr/>		
$+1210.66666666666666 x^6 d^4$	$-479.99999999999999 x^6 d^5$	$+63.99999999999999 x^6 d^6$
<hr/>		
$+1000.02539682539 x^7 d^1$	$+2374.39999999999999 x^7 d^2$	$+2408.53333333333333 x^7 d^3$
<hr/>		
$-4704.0000000000 x^7 d^4$	$+3690.66666666666666 x^7 d^5$	$-1152.0000000000 x^7 d^6$
<hr/>		
$+128.0000000000 x^7 d^7$		
<hr/>		
$-31435.219047619 x^8 d^1$	$+21442.41269841 x^8 d^2$	$-20110.4000000000 x^8 d^3$
<hr/>		
$+12771.2000000000 x^8 d^4$	$-18143.9999999999 x^8 d^5$	$+10495.9999999999 x^8 d^6$
<hr/>		
$-2687.9999999999 x^8 d^7$		$+255.9999999999 x^8 d^8$
<hr/>		
$-20387.53298060 x^9 d^1$	$+294403.1746032 x^9 d^2$	$-95832.1693122 x^9 d^3$
<hr/>		
$+21440.00000000 x^9 d^4$	$+61560.8888888888 x^9 d^5$	$-62080.00000000 x^9 d^6$
<hr/>		
$+28373.333333 x^9 d^7$		$-6144.00000000 x^9 d^8$
<hr/>		
$+512.0000000000 x^9 d^9$		
<hr/>		
$+2051214.7843386 x^{10} d^1$	$-6192978.8227 x^{10} d^2$	$+3181210.20952 x^{10} d^3$
<hr/>		
$-1079716.757669 x^{10} d^4$	$-48661.333333 x^{10} d^5$	$+257267.199999 x^{10} d^6$
<hr/>		
$-195840.000000 x^{10} d^7$	$+73813.333333 x^{10} d^8$	$-13824.000000 x^{10} d^9$
<hr/>		
$+1024.000000 x^{10} d^{10}$		
<hr/>		
$-2725463.2041 x^{11} d^1$	$+18390206.21 x^{11} d^2$	$+2845075.7280 x^{11} d^3$
<hr/>		
$+798591.1877 x^{11} d^4$	$-340330.5315 x^{11} d^5$	$-554547.199 x^{11} d^6$
<hr/>		
$+961186.1329 x^{11} d^7$	$-582143.999 x^{11} d^8$	$+186367.999 x^{11} d^9$
<hr/>		
$-30719.999 x^{11} d^{10}$		$+2047.9999 x^{11} d^{11}$
<hr/>		
$-52046138.6 x^{12} d^1$	$+64425096.1 x^{12} d^2$	$-314627076.1 x^{12} d^3$
<hr/>		
$+126856674.2 x^{12} d^4$	$-20441160.8 x^{12} d^5$	$-520014.1 x^{12} d^6$
<hr/>		
$-3007795.2 x^{12} d^7$	$+3301421 x^{12} d^8$	$-1653248 x^{12} d^9$
<hr/>		
$+459434 x^{12} d^{10}$		$-67584.0 x^{12} d^{11}$
<hr/>		
$+4096.00 x^{12} d^{12}$		
<hr/>		
$-2052218007 x^{13} d^1$	$+563481178e1 x^{13} d^2$	$-20936942e2 x^{13} d^3$
<hr/>		
$+846300080 x^{13} d^4$	$-15546990e1 x^{13} d^5$	$+318945e2 x^{13} d^6$
<hr/>		
$+2724596 x^{13} d^7$	$-1300363e1 x^{13} d^8$	$+1063195e1 x^{13} d^9$
<hr/>		
$-45281e2 x^{13} d^{10}$	$+1110e3 x^{13} d^{11}$	$-147456 x^{13} d^{12}$
<hr/>		
$+8192.0 x^{13} d^{13}$		
<hr/>		

well concentrated along a distinct line for each series, examples of which follow below. But for other series, the Dlog-Padé method, even in combination with an Euler-transformation, is insufficient for a quantitative analysis. So our strategy is in general to use the Dlog-Padé method only to get rough estimates for the critical parameters, as a starting point for a detailed analysis with M1 and M2, and to assess the general behavior of the series from the number of pole-residue pairs which are obtained.

**7.2 Estimation of  $x_c$  and the critical exponents using M1 and M2**

The analysis algorithms M1 and M2 allow the accurate simultaneous determination of the threshold  $x_c$ , the leading critical exponent  $\gamma$ , and the confluent correction to scaling exponent  $\Delta_1$ , assuming the asymptotic form

$$\chi(x) \sim A(x_c - x)^{-\gamma}(1 + B(x_c - x)^{\Delta_1}). \quad (77)$$

**Table 3.** Series for the Uniform distribution on the  $d$ -dimensional hyper-cubic lattice and for  $x = (J/k_{\text{B}}T)^2$ .

Terms of the series. $\chi_{\text{EA}} = 1 + \dots$		
+0.66666666666666666666666666666666 $x^1 d^1$		
-0.4888888888888888888888888 $x^2 d^1$	+0.4444444444444444444444444 $x^2 d^2$	
+0.359788359788359788 $x^3 d^1$	-0.65185185185185185 $x^3 d^2$	+0.296296296296296296 $x^3 d^3$
+0.08084656084656084 $x^4 d^1$	+0.373051146384479718 $x^4 d^2$	-0.65185185185185185 $x^4 d^3$
+0.19753086419753086 $x^4 d^4$		
-0.89147987814654481 $x^5 d^1$	+0.84242210464432686 $x^5 d^2$	+0.49683715461493239 $x^5 d^3$
-0.57942386831275720 $x^5 d^4$	+0.13168724279835391 $x^5 d^5$	
+1.0637968983789089 $x^6 d^1$	-1.862678750213141 $x^6 d^2$	+0.59106251224769744 $x^6 d^3$
+0.60287673917303544 $x^6 d^4$	-0.48285322359396431 $x^6 d^5$	+0.08779149519890260 $x^6 d^6$
+1.255336691527167 $x^7 d^1$	-1.283045789797112 $x^7 d^2$	-0.625225076837070 $x^7 d^3$
+0.3268519171729049 $x^7 d^4$	+0.6538376118623032 $x^7 d^5$	-0.3862825788751715 $x^7 d^6$
+0.0585276634659350 $x^7 d^7$		
-2.764322363362706 $x^8 d^1$	+5.381812025290449 $x^8 d^2$	-1.970220360622241 $x^8 d^3$
-1.100189850013248 $x^8 d^4$	+0.06329348749101851 $x^8 d^5$	+0.6510505802686874 $x^8 d^6$
-0.300442005791800 $x^8 d^7$	+0.03901844231062340 $x^8 d^8$	
-9.85782657798808 $x^9 d^1$	+17.54278833330664 $x^9 d^2$	-9.714423500532811 $x^9 d^3$
+3.026748425908237 $x^9 d^4$	-1.234630286704749 $x^9 d^5$	-0.168708312466884 $x^9 d^6$
+0.608947822994459 $x^9 d^7$	-0.22890819488898 $x^9 d^8$	+0.0260122948737485 $x^9 d^9$
+15.5044273681052 $x^{10} d^1$	-38.7783044835667 $x^{10} d^2$	+33.5641685051471 $x^{10} d^3$
-12.0316553472705 $x^{10} d^4$	+2.84533673882951 $x^{10} d^5$	-1.14514652844366 $x^{10} d^6$
-0.348044505410769 $x^{10} d^7$	+0.543557868404698 $x^{10} d^8$	-0.171681146166746 $x^{10} d^9$
+0.0173415299158332 $x^{10} d^{10}$		
+108.085493498972 $x^{11} d^1$	-232.015426078230 $x^{11} d^2$	+168.045218530949 $x^{11} d^3$
-48.1504957504608 $x^{11} d^4$	+2.24480229556376 $x^{11} d^5$	+2.83058482344332 $x^{11} d^6$
-0.924877616717460 $x^{11} d^7$	-0.467778685821369 $x^{11} d^8$	+0.468089181785302 $x^{11} d^9$
-0.127171219382772 $x^{11} d^{10}$	+0.0115610199438887 $x^{11} d^{11}$	
-142.76066452364 $x^{12} d^1$	+418.50354734964 $x^{12} d^2$	-458.98712418598 $x^{12} d^3$
+231.20946538453 $x^{12} d^4$	-49.940080322749 $x^{12} d^5$	+0.060628792921663 $x^{12} d^6$
+2.7869356691639 $x^{12} d^7$	-0.64727598233428 $x^{12} d^8$	-0.531744115759476 $x^{12} d^9$
+0.39186352362185 $x^{12} d^{10}$	-0.093258894214093 $x^{12} d^{11}$	+0.0077073466292662 $x^{12} d^{12}$
-1391.033864136 $x^{13} d^1$	+3401.571257928 $x^{13} d^2$	-3040.190268119 $x^{13} d^3$
+1234.36058382 $x^{13} d^4$	-211.0538211516 $x^{13} d^5$	+5.814822817330 $x^{13} d^6$
-1.45093243110 $x^{13} d^7$	+2.63953125141 $x^{13} d^8$	-0.365539203648 $x^{13} d^9$
-0.5497466842 $x^{13} d^{10}$	+0.32066232142 $x^{13} d^{11}$	-0.0678246503365 $x^{13} d^{12}$
+0.005138231086 $x^{13} d^{13}$		

In M1, one studies the logarithmic derivative of

$$F(x) = \gamma\chi(x) - (x_c - x)\frac{d\chi(x)}{dx} \quad (78)$$

which has a pole at  $x_c$  with residue  $-\gamma + \Delta_1$ . For a given trial value of  $x_c$  one obtains graphs of  $\Delta_1$  versus  $\gamma$  for all Padé approximants of  $F$ , and chooses the triplet  $x_c, \gamma, \Delta_1$  for which best convergence of the different approximants results [27].

In the M2 method one first transforms the series in  $x$  into series in the variable  $y = 1 - (1 - x/x_c)^{\Delta_1}$  and then

takes Padé approximants to

$$G(y) = \Delta_1(y - 1)\frac{d \ln \chi}{dy} \quad (79)$$

which should converge to  $-\gamma$ . Here one plots graphs of  $\gamma$  versus the input  $\Delta_1$  for different trial values of  $x_c$  and again chooses the triplet  $x_c, \gamma, \Delta_1$  with the best convergence of all Padé approximants. For both methods it is advisable to perform first the usual Dlog-Padé analysis, to get rough estimates of  $x_c$  and  $\gamma$  which one uses as starting points for the detailed analysis with M1 and M2. The

**Table 4.** Series for the Double-Triangular distribution on the  $d$ -dimensional hyper-cubic lattice and for  $x = (J/k_B T)^2$ .

Terms of the series. $\chi_{EA} = 1 + \dots$		
$+1 x^1 d^1$		
$-0.9444444444444444 x^2 d^1$		$+1 x^2 d^2$
$+0.8833333333333333 x^3 d^1$	$-1.8888888888888888 x^3 d^2$	$+0.9999999999999999 x^3 d^3$
$+0.925282186948853615 x^4 d^1$	$+0.908641975308641977 x^4 d^2$	$-2.8333333333333333 x^4 d^3$
$+1.0000000000000000 x^4 d^4$		
$-6.21639476778365667 x^5 d^1$	$+7.16815696649029982 x^5 d^2$	$+1.82592592592592591 x^5 d^3$
$-3.7777777777777777 x^5 d^4$	$+0.9999999999999999 x^5 d^5$	
$+6.3863053214177552 x^6 d^1$	$-15.004896629433666 x^6 d^2$	$+8.705647658240250 x^6 d^3$
$+3.63518518518518 x^6 d^4$	$-4.722222222222222 x^6 d^5$	$+0.9999999999999999 x^6 d^6$
$+31.28590186111328 x^7 d^1$	$-41.38286394727488 x^7 d^2$	$-1.768129041740152 x^7 d^3$
$+10.19533313737017 x^7 d^4$	$+6.336419753086420 x^7 d^5$	$-5.666666666666666 x^7 d^6$
$+1.0000000000000000 x^7 d^7$		
$-42.9465436061225 x^8 d^1$	$+105.962396480164 x^8 d^2$	$-61.3217767001924 x^8 d^3$
$-16.807385633723 x^8 d^4$	$+10.7947922790515 x^8 d^5$	$+9.92962962962962 x^8 d^6$
$-6.611111111111111 x^8 d^7$	$+0.9999999999999999 x^8 d^8$	
$-447.38013758662 x^9 d^1$	$+826.325405622926 x^9 d^2$	$-441.151661966652 x^9 d^3$
$+80.2235926358573 x^9 d^4$	$-35.5380623053978 x^9 d^5$	$+9.66160395845584 x^9 d^6$
$+14.4148148148148 x^9 d^7$	$-7.555555555555555 x^9 d^8$	$+1.0000000000000000 x^9 d^9$
$+331.676191097529 x^{10} d^1$	$-1222.22773822861 x^{10} d^2$	$+1383.83407091038 x^{10} d^3$
$-545.353553191950 x^{10} d^4$	$+91.7181421721279 x^{10} d^5$	$-57.8924350055523 x^{10} d^6$
$+5.95334705075442 x^{10} d^7$	$+19.7919753086420 x^{10} d^8$	$-8.500000000000000 x^{10} d^9$
$+1.0000000000000000 x^{10} d^{10}$		
$+10066.680607773 x^{11} d^1$	$-22331.632875336 x^{11} d^2$	$+16898.722229737 x^{11} d^3$
$-5104.9579819064 x^{11} d^4$	$+412.40450343047 x^{11} d^5$	$+125.3464089002 x^{11} d^6$
$-83.007159731749 x^{11} d^7$	$-1.1723995688801 x^{11} d^8$	$+26.061111111110 x^{11} d^9$
$-9.444444444444 x^{11} d^{10}$	$+0.99999999999998 x^{11} d^{11}$	
$-1250.8803969425 x^{12} d^1$	$+16566.72572040 x^{12} d^2$	$-31549.37183747 x^{12} d^3$
$+21664.50242641 x^{12} d^4$	$-5879.76957662 x^{12} d^5$	$+360.0325939430 x^{12} d^6$
$+186.7090665165 x^{12} d^7$	$-109.223272530 x^{12} d^8$	$-12.5580570252 x^{12} d^9$
$+33.22222222221 x^{12} d^{10}$	$-10.38888888888 x^{12} d^{11}$	$+0.999999999999 x^{12} d^{12}$
$-288282.12879 x^{13} d^1$	$+726711.250361 x^{13} d^2$	$-676798.593987 x^{13} d^3$
$+289743.600575 x^{13} d^4$	$-53400.7324666 x^{13} d^5$	$+1584.74112371 x^{13} d^6$
$+292.731945980 x^{13} d^7$	$+281.321506576 x^{13} d^8$	$-134.086189495 x^{13} d^9$
$-29.046046443 x^{13} d^{10}$	$+41.2753086420 x^{13} d^{11}$	$-11.3333333333 x^{13} d^{12}$
$+1.000000000000 x^{13} d^{13}$		

effectiveness and preciseness of these series analysis methods has been demonstrated in several papers [26, 28–30].

In M1 we vary the trial- $x_c$  until the curves from the high order Padé approximants enter fairly symmetrically from both sides and the best convergence is obtained. This  $x_c$  and the corresponding  $\gamma$  are taken as the temporary best estimates for that series, with temporary error estimates from the nearest trial- $x_c$ 's, whose plots show poorer convergence. In many cases M1 proves to be quite sensitive to small changes in the trial- $x_c$ , and the degree of convergence usually looks very convincing. Away from the best  $x_c$ , convergence degrades quickly, the picture becomes non-symmetric and at the same time the area of

convergence shifts to lower or higher values of  $\gamma$ . We show examples of such plots in Section 7.4. In M2 we vary  $x_c$  and look for best convergence of the Padé approximant curves while they cross each other with a small negative slope. Compared to M1, the M2-plots are often much less decisive. A good convergence region sustains over a wider range, where again the change in  $x_c$  is accompanied by a shift in the corresponding  $\gamma$ .

In the end we determine an overall estimate for  $x_c$ , which is consistent with the estimates from both M1 and M2. These numerical results are presented in the tables of Section 7.4. In the tables we also include rough estimates for  $\Delta_1$ . We comment that the Euler transformation

**Table 5.** Results for dimension  $d = 8$  from the analysis with Dlog-Padé, M1 and M2. The first line for each distribution shows the result from the Dlog-Padé analysis in which Euler transformations with different values  $x_n$  were used. The remaining lines show the results from M1 in combination with M2, separately for several values of  $x_n$ .

Distribution	Parameter $x_n$	Threshold $x_c$	Exponent $\gamma$	Correction- Exponent
Bimodal	several	0.072	1.05(1)	n/a
	-0.084	0.07331(3)	1.046(9)	1.4-1.7
	-0.073	0.07331(3)	1.046(9)	1.4-1.7
	-0.056	0.07332(3)	1.047(12)	1.3-1.5
Gaussian	several	0.080	1.068(20)	n/a
	-0.084	0.08030(3)	1.048(9)	1.3-1.5
	-0.070	0.08029(3)	1.047(12)	1.3-1.5
	-0.056	0.08030(3)	1.048(9)	1.3-1.5
Double-Triangular	several	0.148	1.072(22)	n/a
	-0.168	0.14895(3)	1.048(9)	1.3-1.7
	-0.140	0.14895(3)	1.048(9)	1.3-1.5
Uniform	-0.112	0.14898(9)	1.048(9)	1.3-1.5
	several	0.228	1.069(25)	n/a
	-0.252	0.22852(9)	1.048(6)	1.3-1.5
	-0.210	0.22848(6)	1.048(6)	1.3-1.5
	-0.168	0.22854(9)	1.048(6)	1.3-1.5

is known to produce analytic correction terms even if not present originally. When the leading correction exponent is larger than 1, as seems to be the case for some of our series, these ‘artificial’ corrections will show up in M1 and M2 [31], and hence our  $\Delta_1$  estimates are mainly included for reference and should not be trusted as the real physical values.

### 7.3 Sensitivity to the parameter of the Euler transformation

Our analysis relies in a large part on the use of Euler transformations to increase the number of useful Padé approximants and to improve their convergence. The technique is well established and has been used with success [32], but nevertheless we find it worthwhile to check, to what degree our results are sensitive to the precise choice of the parameter  $x_n$ , the value of  $x$  that is mapped to infinity by the transformation. We first choose  $x_n$  very close to the negative singularity, as indicated by the Dlog-Padé analysis of the original series. We then vary this  $x_n$  over a considerable range of typically 20%, and compare the results. We observe that a variation of  $x_n$  *does* move the data points or curves obtained from individual Padé approximants, but that the average (in Dlog-Padé plots) and the convergence region (in M1 plots) stay fixed to a very good accuracy, when compared to the error bounds given by the analysis technique itself. We thus exclude that our results are artifacts of the applied Euler transformations.

### 7.4 Explicit results from the analysis

The numerical results for dimension 8 are summarized in Table 5. In this dimension, even without an Euler transformation, the Dlog-Padé analysis gives convincing results

for all the distributions: Bimodal, double-triangular, uniform and Gaussian.

During the analysis we prepared a large number of plots of which we can only present a few to illustrate the process. The distribution of the pole-estimates indicates a negative real pole for the asymptotic function, somewhat weaker than the positive one (e.g. Fig. 3). Both poles are at the same distance from the origin. The convergence of pole-residue pairs improves upon Euler transformation.

The numerical results for the critical exponents are calculated as averages over estimates from high-order Padé approximants. These include data from the untransformed series and from the series transformed with three different values of  $x_n$ . In the tables these are the entries without an estimate for  $\Delta_1$ . All values are slightly larger than the mean field value of  $\gamma = 1$  (Fig. 4). This deviation is understood on theoretical grounds as being due to corrections to the leading singular behavior. Also the data indicate that the exponent estimate may further approach 1 for longer series, since generally residues decrease in value as the approximant-order increases while remaining greater than one (Fig. 5). When taking into account the correction exponent with M1/M2 the deviation also decreases. The results from M1 and M2 are shown in the table separately for different values of  $x_n$ , and generally show very good agreement. We observe the possibility of a systematic shift to  $\gamma = 1.060(12)$  in case one chooses a different region of best convergence. The values for  $\Delta_1$  are included for reference only, due to the reason mentioned before. Although the absolute value of the exponent-estimate is larger than 1, we find numerical agreement of the results for all the tested distributions.

The qualitative behavior in dimension 7 agrees with that for  $d = 8$ , although the exponent estimates are slightly farther away from 1 (see Tab. 6). The critical threshold  $x_c$  for each series is larger than in dimension 8. Again we observe a negative pole of comparable strength

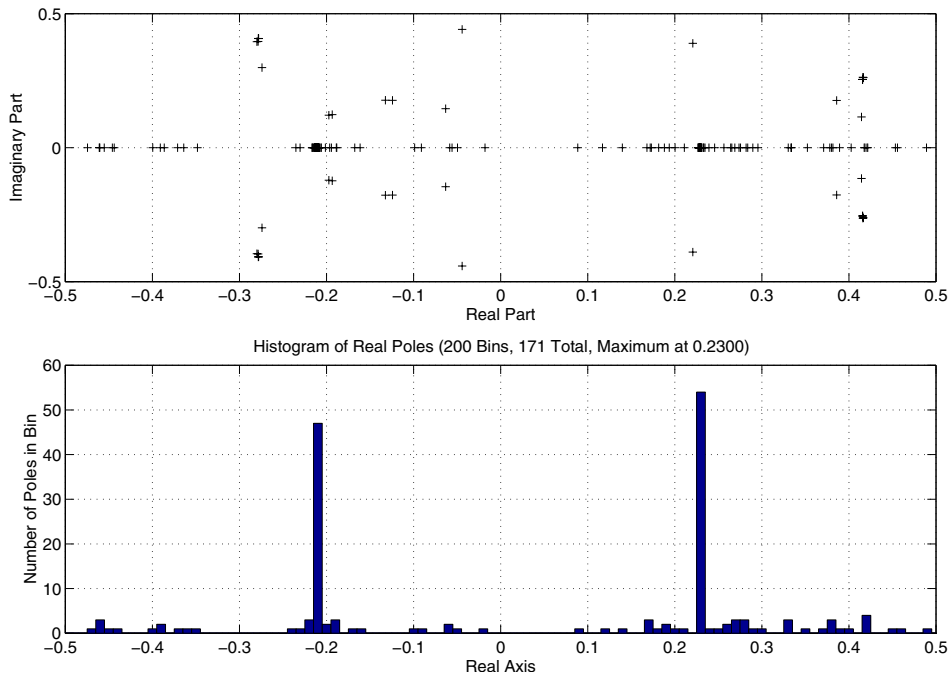


**Fig. 3.** Position of the poles from all Padé approximants to the logarithmic derivative of the untransformed series of  $\chi_{EA}$  for the uniform distribution in  $d = 8$ . The upper half shows the location of the poles in the complex plane. The lower part is a histogram of the poles along the real axis, in which the two peaks are of relevance. The one on the positive axis represents the physical singularity we want to characterize, the second one can interfere with analysis and may be mapped away using an Euler transformation.

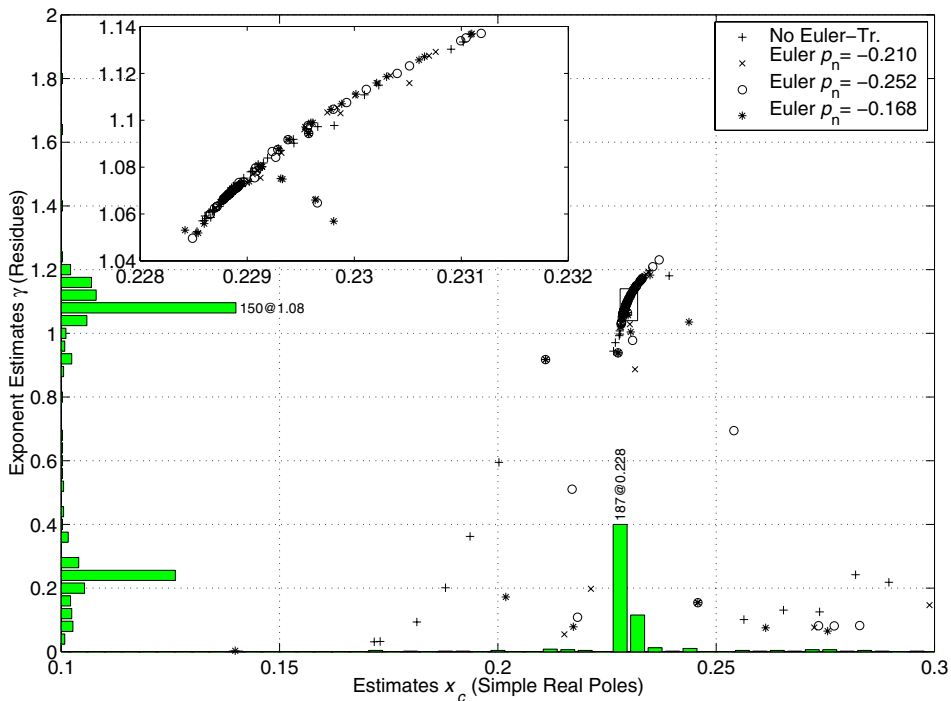


**Fig. 4.** Pole-residue plot from a Dlog Padé analysis of the  $\chi_{EA}$ -series for the uniform distribution in  $d = 8$ . We use Euler transformations with several values  $p_n$ . The main part gives an overview over a large region including almost all data points. The inset is an enlarged view of the small region with the highest concentration of points as indicated by the box. For comparison we calculate the average and standard deviation  $\sigma_n$  from the points in the boxed area.



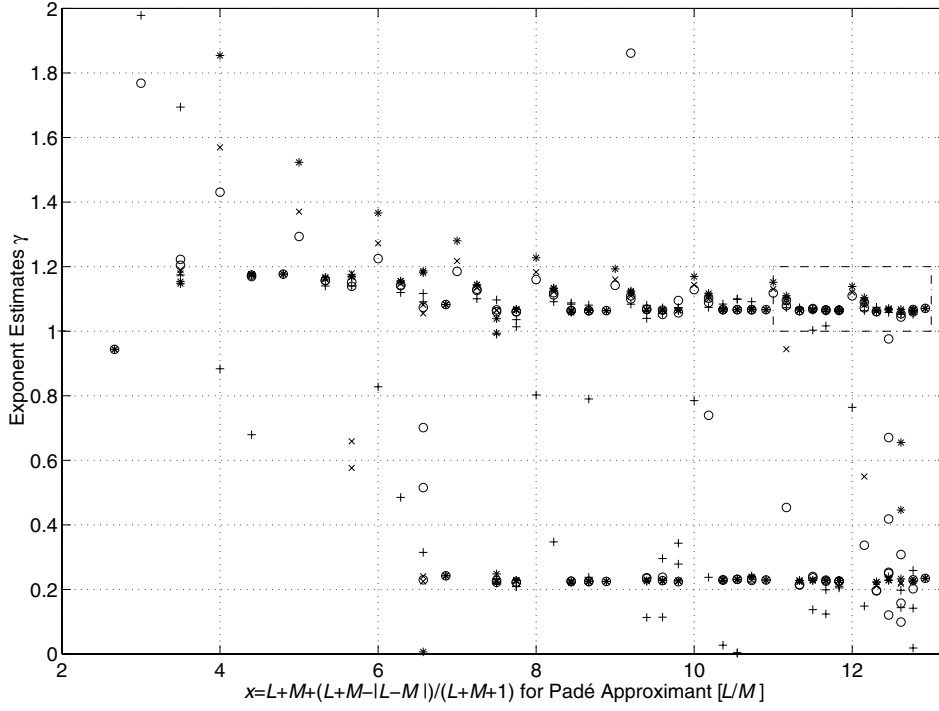


**Fig. 5.** Estimates for the leading critical exponent  $\gamma$  from the  $\chi_{EA}$ -series for the double-triangular distribution in  $d = 8$ . Series transformed with different values for  $x_n$ , indicated by different symbols, contribute to the plot. Each point corresponds to a particular transformation and Padé approximant  $[L/M]$ , where  $L$  and  $M$  relate to the number on the  $x$ -axis as given in the label. The different symbols refer to different parameters for the Euler transformation: Without (+),  $x_n = -0.140$  ( $\times$ ),  $x_n = -0.168$  ( $\circ$ ), and  $x_n = -0.112$  (\*). Estimates are calculated as averages over points in the convergence region. The points that are included in the average are those within the boxed area. The resulting numbers, in this case of  $\gamma = 1.07 \pm 0.02$ , enter Table 5.

**Table 6.** Results for dimension  $d = 7$  from the analysis with Dlog-Padé, M1 and M2. The first line for each distribution shows the result from the Dlog-Padé analysis in which no Euler transformations was applied. The remaining lines show the results from M1 in combination with M2, separately for several values of  $x_n$ .

Distribution	Parameter $x_n$	Threshold $x_c$	Exponent $\gamma$	Correction-Exponent
Bimodal	none	0.088	1.14(3)	n/a
	-0.082	0.08731(9)	1.105(15)	1.5-1.7
	-0.078	0.08732(9)	1.105(12)	1.3-1.7
	-0.051	0.08738(6)	1.110(15)	1.3-1.4
Gaussian	none	0.097(1)	1.14(3)	n/a
	-0.071	0.09710(6)	1.107(9)	1.3-1.4
	-0.062	0.09712(9)	1.108(12)	$\approx 1.3$
Double-Triangular	none	0.1784(4)	1.14(3)	n/a
	-0.265	0.17790(9)	1.108(9)	1.3-1.6
	-0.156	0.17790(9)	1.108(9)	1.3-1.5
	-0.112	0.17799(9)	1.110(6)	$\approx 1.3$
Uniform	none	0.2745(5)	1.13(3)	n/a
	-0.315	0.27402(9)	1.108(9)	1.3-1.5
	-0.234	0.27399(9)	1.108(6)	1.3-1.5
	-0.225	0.27399(9)	1.108(6)	1.3-1.5

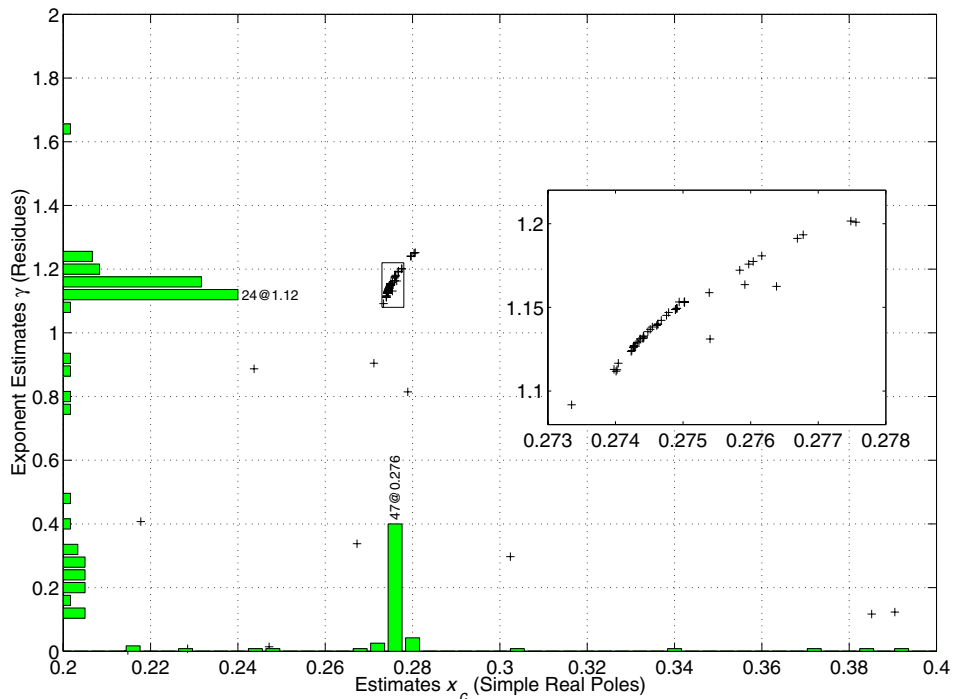


**Fig. 6.** Pole-residue plot from a Dlog Padé analysis of the untransformed  $\chi_{EA}$ -series for the Uniform distribution in  $d = 7$ . See the caption of Figure 4 for further explanation.

and distance from the origin as the physical one, but nevertheless, even without an Euler transformation the series give consistent results. To illustrate this we show in Figure 6 a pole-residue plot of the untransformed series for the uniform distribution and also include in Table 6 the estimates from the Dlog-Padé analysis without transformation. In our M1/M2-analysis we again observe the possibility of a systematic shift to  $\gamma = 1.120(15)$  in case one chooses a different region of best convergence.

In dimension 5 the negative pole is closer to the origin than the positive one, and convergence degrades. Still the data points line up properly. To improve their convergence and to get higher numerical accuracy we apply Euler transformations with several  $x_n$  (e.g. Fig. 7) and the final estimates (Tab. 7) are obtained the same way as described before. Looking at Figure 8, the main line of data-points for the Gaussian distribution still increases with the order of the Padé approximants. Therefore, the value measured by this method is probably smaller than what a longer series would show. In summary, all studied distributions agree at  $d = 5$  on a common exponent within their error margins.

In Figures 9 to 10 we show, for the case of the Gaussian distribution, plots as they are typically obtained from M1. Each curve in a plot comes from a different Padé approximant as the legend shows. In all figures we clearly see a region where the lines converge, and since all figures show the same range in the  $\gamma$ - $\Delta_1$ -plane it is also easy to see that the convergence region shifts around. Figures 9a and b differ in the trial  $x$  as input parameter. While for  $x = 0.177$

convergence is quite good, it becomes better for  $x = 0.179$  (in fact best among our trial values). At this value of  $x$  the shape of the curves is also symmetric and they switch over to one side for larger  $x$  (the opposite side, when compared to the smaller  $x$ ) which we find to be a characteristic feature of the point of best convergence. Figure 10 shows the corresponding plot for the untransformed series. Here  $x = 0.179$  is also near the characteristic point of symmetric curves. Still convergence is not as good as in Figure 9b and the center is shifted to a slightly larger value of  $\gamma$ . The example, although not the most common case, also illustrates that one must not rely on analysis with either M1 or M2 alone. While M1 gives an estimate of  $\gamma = 2$  or higher, M2 (Fig. 11) points to a lower value of roughly 1.82 and  $\Delta_1$  above 1, or  $\gamma \approx 1.95$  with  $\Delta_1$  below 1 and poorer convergence. Our estimates in the tables always result from using M1 together with M2. Figure 12 is another example, showing a plot from M1-analysis for the Uniform distribution near the symmetry point of best convergence.

As we decrease the dimension further to  $d = 4$ , the analysis becomes increasingly difficult. One reason is the negative pole on the real axis, which is very strong and apparent for all the series. Without an Euler transformation, the Dlog-Padé analysis does not show anything conclusive. For the transformed series, a larger number of data points lines up well in the pole-residue plots, but they are still not well converged. The series for the Gaussian distribution is somewhat exceptional here: Exponent estimates converge well with increasing approximant-order, but they approach a value of  $\gamma = 3.1 \pm 0.1$  which is much

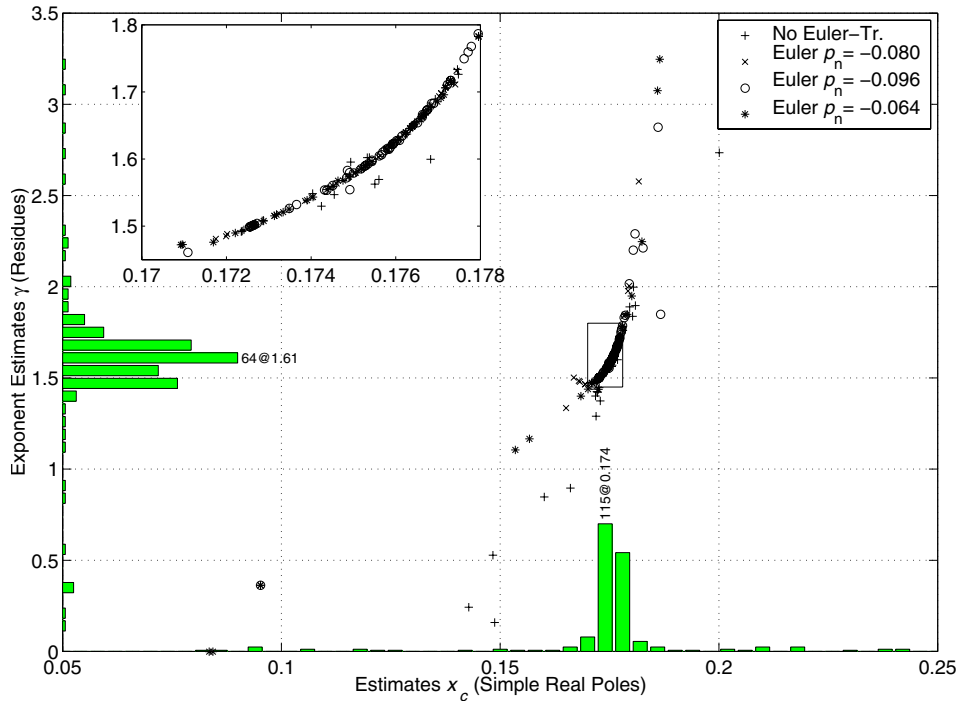


**Fig. 7.** Pole-residue plot from a Dlog Padé analysis of the  $\chi_{EA}$ -series for the Gaussian distribution in  $d = 5$ . We use Euler transformations with several values  $p_n$ . See the caption of Figure 4 for further explanation.

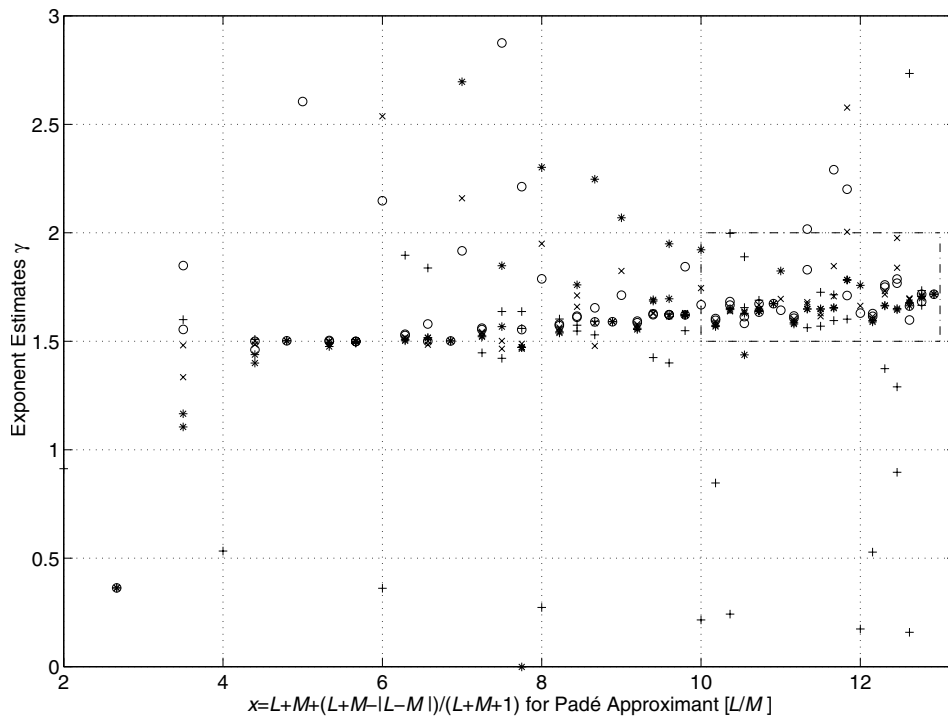


**Fig. 8.** Estimates for the leading critical exponent  $\gamma$  from the  $\chi_{EA}$ -series for the Gaussian distribution in  $d = 5$ . See the caption of Figure 5 for details. The distribution of the data-points indicates that the  $\gamma$ -estimate may still increase with longer series. The different symbols refer to different parameters for the Euler transformation: Without (+),  $x_n = -0.080$  (x),  $x_n = -0.096$  (o), and  $x_n = -0.064$  (\*). Averaging over the points inside the small box leads to an estimate of  $\gamma = 1.68 \pm 0.08$ , which enters Table 7.

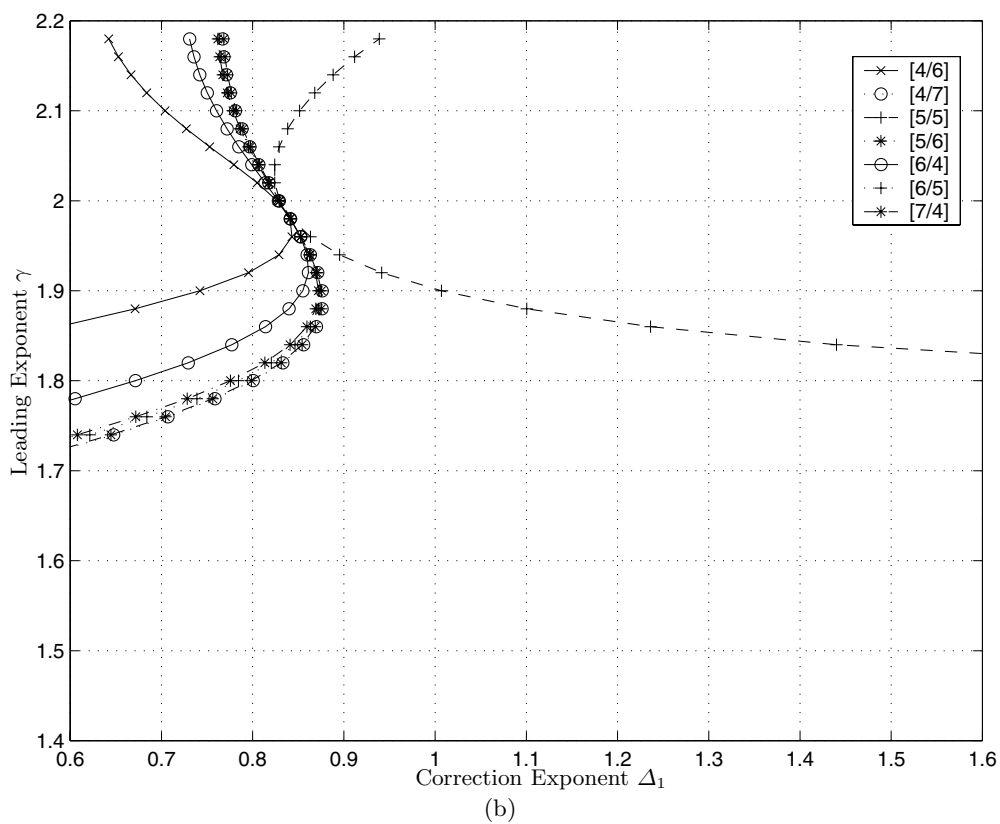
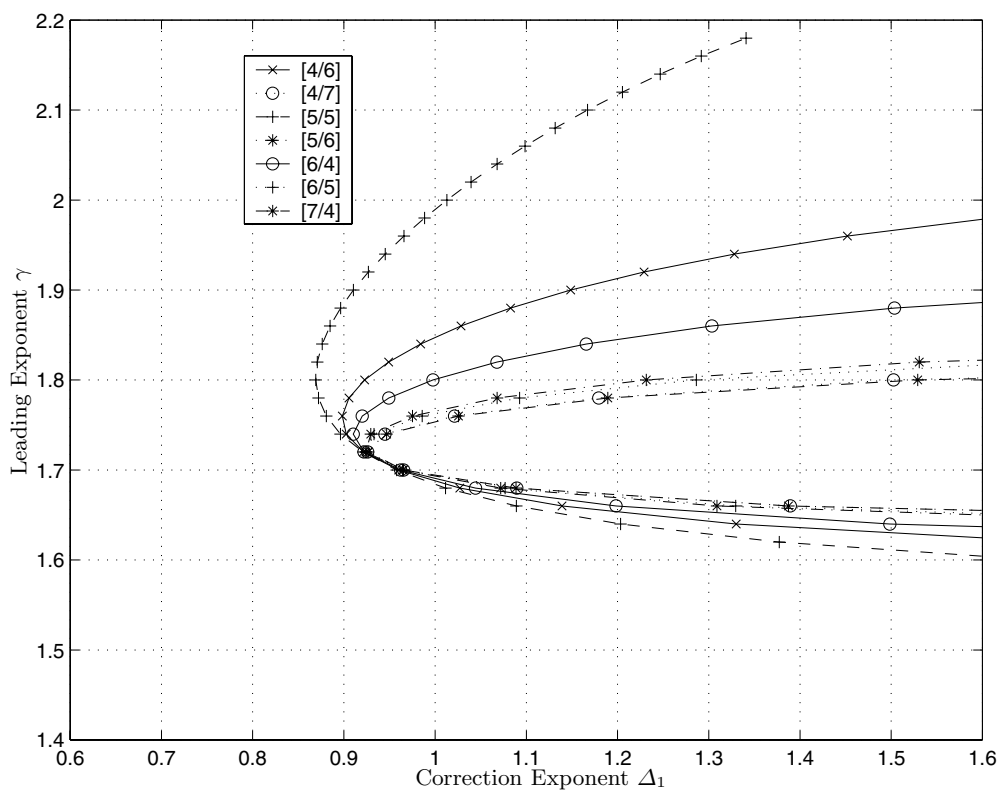


**Fig. 9.** M1 analysis of the  $\chi_{\text{EA}}$ -series for the Gaussian distribution in  $d = 5$ . An Euler transformation with  $x_n = 0.08$  was applied. Plot (a) was obtained for a trial  $x$  of 0.177, where convergence is visible but lies below the optimal convergence point. In (b) the trial  $x = 0.179$  is near or at the point of optimal convergence.

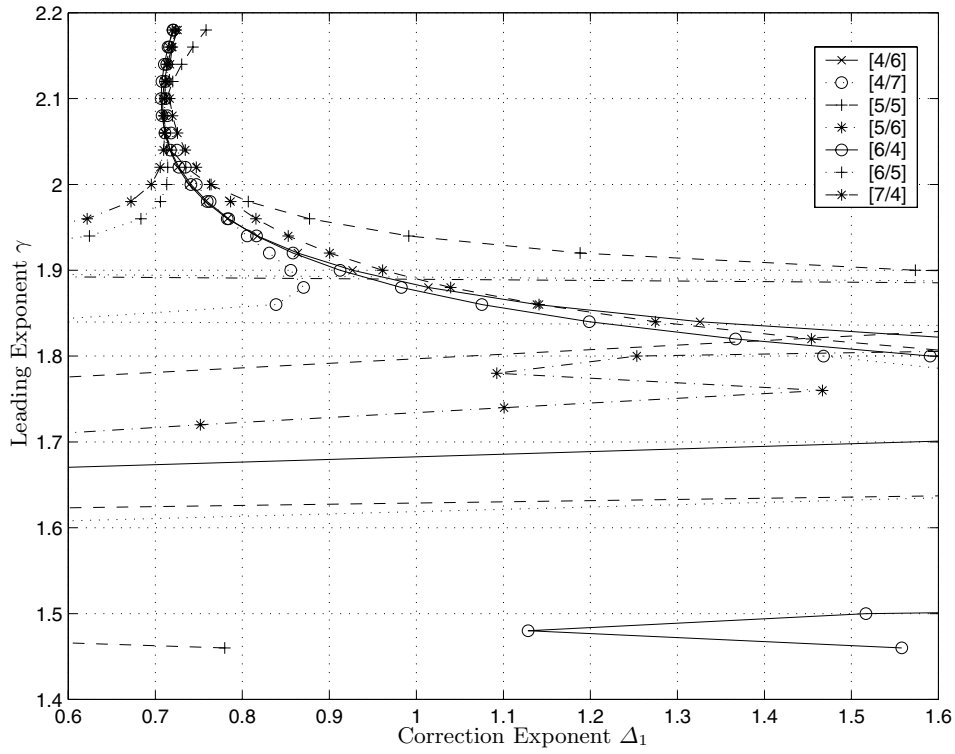


**Fig. 10.** M1 analysis of the untransformed  $\chi_{EA}$ -series for the Gaussian distribution in  $d = 5$ . The trial  $x = 0.179$  is near or at the point of optimal convergence. Compared to Figure 9(b), with Euler-transformation, convergence is less sharp and shifted to a slightly larger  $\gamma$ . Strong fluctuations of the Padé-lines are visible in the lower part of the plot.

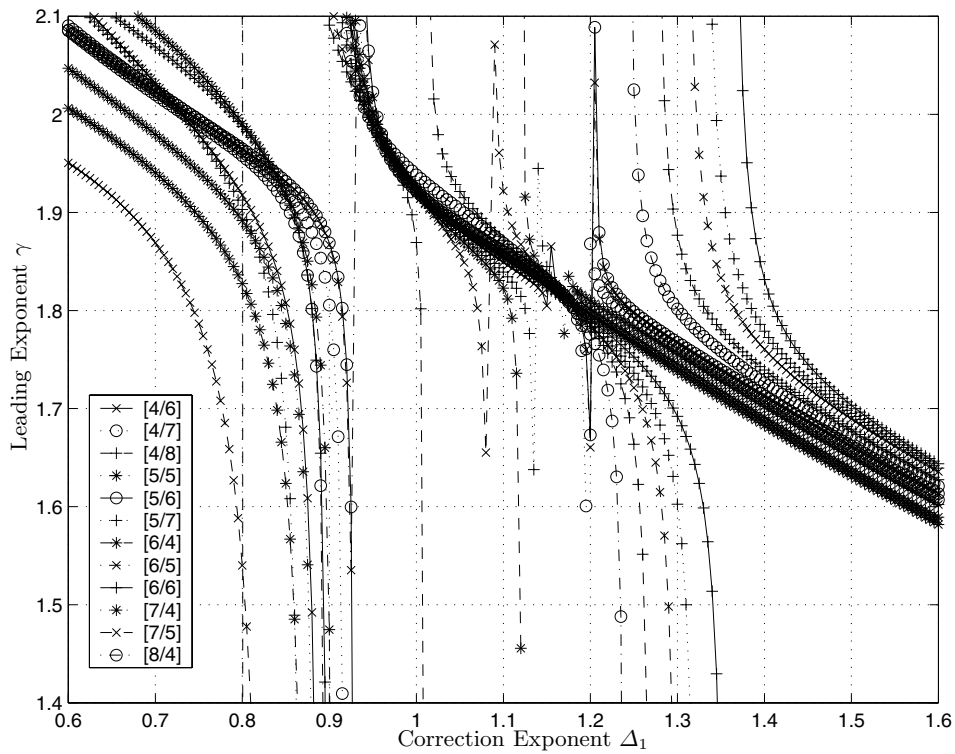


**Fig. 11.** M2 analysis of the Euler-transformed  $\chi_{EA}$ -series ( $x_n = 0.08$ ) for the Gaussian distribution in  $d = 5$  and for a trial  $x$  of 0.179. Illustrates the need to use M1 and M2 in combination.

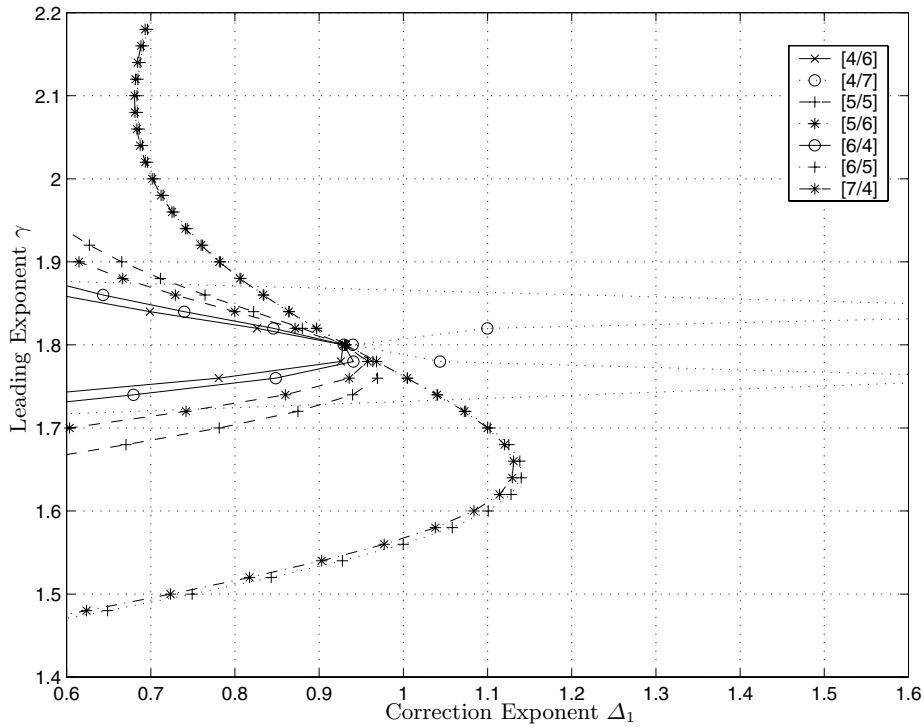


**Fig. 12.** M1 analysis of the  $\chi_{EA}$ -series for the uniform distribution in  $d = 5$ , after an Euler-transformation with  $x_n = 0.29$ .  $x = 0.488$  is near or at the the point of optimal convergence.

**Table 7.** Results for dimension  $d = 5$  from the analysis with Dlog-Padé, M1 and M2. See caption of Table 5 for details.

Distribution	Parameter $x_n$	Threshold $x_c$	Exponent $\gamma$	Correction- Exponent
Bimodal	several	0.154	1.91(10)	n/a
	-0.120	0.154(3)	1.95(15)	1.1–1.3
	-0.100	0.154(3)	1.95(15)	$\approx 1.0$
Gaussian	several	0.174	(1.67(8))	n/a
	-0.096	0.176(3)	1.70(15)	0.8–1.0
	-0.080	0.177(3)	1.75(15)	0.8–1.0
	-0.064	0.177(3)	1.75(15)	0.8–1.0
Double- Triangular	several	0.312	1.81(7)	n/a
	-0.240	0.312(6)	1.80(15)	0.9–1.0
	-0.200	0.312(6)	1.80(15)	0.9–1.0
Uniform	several	0.484	1.72(6)	n/a
	-0.348	0.484(6)	1.70(15)	1.0–1.2
	-0.290	0.487(6)	1.70(15)	0.8–1.0

higher than what we obtain in the other cases and with the other methods. If this is not simply an artifact of the transformation, it must be attributable to the correction-term to scaling, which becomes increasingly important at lower dimension.

With M1/M2 applied to the transformed series we are able to obtain estimates for  $x_c$  and  $\gamma$ , although the error margins are quite large. Indeed, the value we obtain for the correction exponent  $\Delta_1$  is much larger than 1 (and larger than in the higher dimensions). Again we find that

our numbers agree with a common exponent  $\gamma$  for all the distribution functions.

## 8 Conclusions

Figure 13 summarizes our numerical estimates for the leading critical exponent  $\gamma$  of the Edwards Anderson susceptibility  $\chi_{EA}$  in the different dimensions. For each dimension we show the 4 values obtained for the different

**Table 8.** Results for dimension  $d = 4$  from the analysis with Dlog-Padé, M1 and M2. The table lines without estimates for  $\Delta_1$  stem from the Dlog-Padé analysis in which Euler transformations with different values  $x_n$  were used. The remaining lines show the results from M1 in combination with M2, separately for several values of  $x_n$ .

Distribution	Parameter $x_n$	Threshold $x_c$	Exponent $\gamma$	Correction- Exponent
Bimodal	-0.144	0.26(2)	2.5(3)	1.5–1.6
	-0.120	0.26(2)	2.5(3)	1.5–1.6
	several	0.31(2)	3.1(1)	n/a
Gaussian	-0.108	0.312(4)	2.3(1)	1.3–1.4
	-0.090	0.314(4)	2.3(1)	1.3–1.4
	-0.072	0.314(4)	2.3(1)	1.3–1.4
Double-Triangular	several	0.52(8)	2.8(8)	n/a
	-0.276	0.54(2)	2.5(2)	$\approx 1.5$
	-0.230	0.54(2)	2.5(2)	$\approx 1.5$
Uniform	-0.396	0.84(2)	2.5(1)	1.3–1.4
	-0.330	0.83(2)	2.4(1)	1.3–1.4
	-0.264	0.84(2)	2.4(1)	1.3–1.4

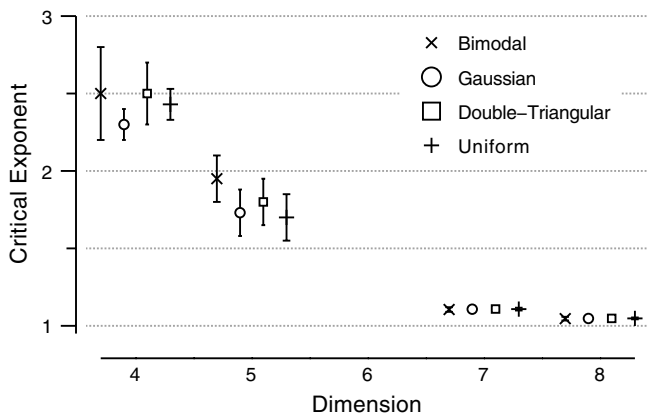


**Fig. 13.** Estimates for the critical exponent  $\gamma$  grouped by space dimension. The different values for each dimension are obtained from the 4 probability distributions. The estimates appear to agree on a common exponent  $\gamma$  within but separately in each dimension. Above the critical dimension  $d_u = 6$  the values are close to 1.

random distributions. The mean values and error bars are as shown in Tables 5 to 8.

The error bars for dimensions 7 and 8 are too small to be visible in the plot. We observe once more that in these dimensions the estimates are close to, but still larger than the expected mean-field value of 1. As we argued, the deviation is likely caused by correction to scaling terms and the fact that we work with relatively short series. Our Dlog-Padé analysis suggests smaller estimates with longer series, and when accounting for the first correction term using the methods M1 and M2 the deviation indeed decreases, but higher order corrections cannot be excluded. The larger deviation for  $d = 7$  is consistent with the observation that the correction terms are more dominant in lower dimensions.

As expected, the estimates we obtain for dimensions 4 and 5 are pronouncedly different from the mean field

value. Within each dimension the estimates agree on a common value for all the random distributions we study, which is roughly  $\gamma = 2.4 \pm 0.2$  in  $d = 4$  and  $\gamma = 1.8 \pm 0.2$  in  $d = 5$ . Thus our data do not indicate that the random distribution for the quenched-in disorder splits the spin glass model into many universality classes nor that the model behaves in that respect differently than other common thermodynamic models, in contrast to claims from references [14–20]. Instead we find confirmation for the established picture, that the space dimension creates universality classes and that the leading critical exponent is a universal quantity [33].

Most of the simulations of the Ising spin glass have been done in dimension 3, in which our series do not perform well. For a direct comparison we are thus limited to the sparse results for  $d = 4$  from [16,18]. Our estimates for the critical temperature  $T_c$  agree rather well with those by Bernardi and Campbell. The compared values are  $T_c = 1.96$  (vs.  $1.99 \pm 0.01$ ) for the bimodal distribution,  $T_c = 1.88$  (vs.  $1.91 \pm 0.01$ ) for the uniform distribution, and  $T_c = 1.79$  (vs.  $1.77 \pm 0.01$ ) for the Gaussian distribution, where the uncertainty in our estimates is also roughly 1 in the last digit, from fluctuations and from possible additional systematic shifts, due to scaling corrections. We confirm a slight decrease of  $T_c$  with increasing kurtosis of the random distributions, which is defined as the ratio of moments  $R = M_4/M_2^2$ . The kurtosis values are: Bimodal 1, double-triangular  $4/3$ , uniform  $9/5$ , Gaussian 3 and for the exponential distribution 6. Bernardi and Campbell have calculated the exponent  $\eta$ , while we have values for  $\gamma$ , so we currently lack a third exponent, such as  $\nu$ , for a direct comparison. However, the discrepancy in the general universal vs. non-universal behavior remains.

Some authors [34–36] have stressed the importance of corrections to finite size scaling (FSS). In taking these into account, they do not find violated universality. We cannot assess the quality of the simulations that were done by Bernardi, Campbell [14–16,19] and others, but, from the data in the papers and later citations, we are led to

speculate that neglected corrections to FSS have caused systematic errors in the exponent estimates from simulations. We would further like to stress the general statement made by other authors, that the characteristic features of the spin glass with its quenched-in disorder creates enormous problems for simulations. Series expansion techniques appear here particularly suitable since the configurational average over the randomness is handled *exactly* within their framework and own limitations.

We thank Ian Campbell for several stimulating communications and the German Israeli Foundation for financial support.

## References

1. S.F. Edwards, P.W. Anderson, *J. Phys. F: Metal Phys.* **5**, 965 (1975)
2. K. Binder, A.P. Young, *Rev. Mod. Phys.* **58**, 801 (1986)
3. K.H. Fisher, J.A. Hertz, *Spin Glasses* (Cambridge University Press, 1991)
4. A.P. Young, *Comp. Phys. Comm.* **146**, 107 (2002)
5. C. Amoruso, E. Marinari, O.C. Martin, A. Pagnani, *Phys. Rev. Lett.* **91**, 087201 (2003)
6. C. de Dominicis, I. Kondor, T. Temesvári, "Beyond the Sherrington-Kirkpatrick Model," in *Spin Glasses and Random Fields*, edited by A.P. Young (World Scientific, Singapore, 1998), pp. 119–160
7. J. Wang, A.P. Young, *J. Phys. A: Math. Gen.* **26**, 1063 (1993)
8. L. Klein, J. Adler, A. Aharony, A.B. Harris, Y. Meir, *Phys. Rev. B* **43**, 11249 (1991)
9. E. Pytte, J. Rudnick, *Phys. Rev. B* **19**, 3603 (1979)
10. R.R.P. Singh, S. Chakravarty, *Phys. Rev. Lett.* **57**, 245 (1986)
11. R.R.P. Singh, *Phys. Rev. Lett.* **67**, 899 (1991)
12. R.E. Hetzel, R.N. Bhatt, R.R.P. Singh, *Europhys. Lett.* **22**, 383 (1993)
13. R.R.P. Singh, J. Adler, *Phys. Rev. B* **54**, 364 (1996)
14. L. Bernardi, I.A. Campbell, *Europhys. Lett.* **26**, 147 (1994)
15. L. Bernardi, I.A. Campbell, *Phys. Rev. B* **49**, 728 (1994)
16. L. Bernardi, I.A. Campbell, *Phys. Rev. B* **52**, 12501 (1995)
17. L.W. Bernardi, S. Prakash, I.A. Campbell, *Phys. Rev. Lett.* **77**, 2798 (1996)
18. L.W. Bernardi, I.A. Campbell, *Phys. Rev. B* **56**, 5271 (1997)
19. L.W. Bernardi, N. Lemke, P.O. Mari, I.A. Campbell, A. Alegria, J. Colmenero, *Physica A* **257**, 21 (1998)
20. I. Campbell, D. Petit, P.O. Mari, L. Bernardi, *J. Phys. Soc. Jpn* **69**, 186 (2000)
21. M.F. Sykes, J.W. Essam, B.R. Heap, B.J. Hiley, *J. Math. Phys.* **7**, 1557 (1966)
22. C.C. Wan, A.B. Harris, J. Adler, *J. Appl. Phys.* **69**, 5191 (1991)
23. D. Daboul, Ph.D. thesis, Tel Aviv University, 2004
24. A.B. Harris, *Phys. Rev. B* **26**, 337 (1982)
25. J.L. Gammel, in *Padé Approximants and Their Applications*, edited by B.R. Graves-Morris (Academic Press, New York, 1973)
26. J. Adler, M. Moshe, V. Privman, *Phys. Rev. B* **26**, 1411 (1982)
27. J. Adler, I. Chang, S. Shapira, *Int. J. Mod. Phys. C: Phys. Comput.* **4**, 1007 (1993)
28. J. Adler, Y. Meir, A. Aharony, A.B. Harris, L. Klein, *J. Stat. Phys.* **58**, 511 (1990)
29. J. Adler, D. Stauffer, *Physica A* **181**, 396 (1992)
30. M. Gofman, J. Adler, A. Aharony, A.B. Harris, M. Schwartz, *Phys. Rev. Lett.* **71**, 1569 (1993)
31. J. Adler, I.G. Enting, *J. Phys. A: Math. Gen.* **17**, 2233 (1984)
32. C.J. Pearce, *Ann. Phys.* **27**, 89 (1978)
33. V. Privman, P.C. Hohenberg, A. Aharony, "Universal Critical-Point Amplitude Ratios," in *Phase Transitions and Critical Phenomena*, edited by C. Domb, M.S. Green, J.L. Lebowitz (Academic Press, New York, 1991), Vol. 14, p. 1
34. N. Kawashima, A.P. Young, *Int. J. Mod. Phys. C: Phys. Comput.* **7**, 327 (1996)
35. H.G. Ballesteros, A. Cruz, L.A. Fernandez, V. Martin-Mayor, J. Pech, J.J. Ruiz-Lorenzo, A. Tarancon, P. Tellez, C.L. Ullod, C. Ungil, *Phys. Rev. B* **62**, 14237 (2000)
36. P.O. Mari, I.A. Campbell, *Phys. Rev. B* **65**, 184403 (2002)